



Calhoun: The NPS Institutional Archive
DSpace Repository

Theses and Dissertations

1. Thesis and Dissertation Collection, all items

2000-05-22

Changing mass applications in an advanced time domain ship motion program

Wynn, Paul Richard

Cambridge, Massachusetts, Massachusetts Institute of Technology

<http://hdl.handle.net/10945/37780>

Downloaded from NPS Archive: Calhoun



Calhoun is a project of the Dudley Knox Library at NPS, furthering the precepts and goals of open government and government transparency. All information contained herein has been approved for release by the NPS Public Affairs Officer.

Dudley Knox Library / Naval Postgraduate School
411 Dyer Road / 1 University Circle
Monterey, California USA 93943

<http://www.nps.edu/library>

Changing Mass Applications in an Advanced Time Domain
Ship Motion Program

by

Paul Richard Wynn

B.S., Virginia Tech (1986)

Submitted to the Department of Ocean Engineering
in partial fulfillment of the requirements for the degree of

Naval Engineer

at the

MASSACHUSETTS INSTITUTE OF TECHNOLOGY

June 2000

© 2000 Paul R. Wynn. All rights reserved.

The author hereby grants to MIT permission to reproduce
and to distribute publicly paper and electronic
copies of this thesis document in whole or in part.


Signature of Author . . .



Department of Ocean Engineering
22 May 2000

Certified by



 Dick K.P. Yue
Professor of Hydrodynamics and Ocean Engineering
Thesis Supervisor

Accepted by



Nicholas M. Patrikalakis
Kawasaki Professor of Engineering
Chairman, Committee on Graduate Students
Department of Ocean Engineering

20000717 044

AD NUMBER	DATE 29 JUNE 2000	DTIC ACCESSION NOTICE
1. REPORT IDENTIFYING INFORMATION		REQUESTER: 1. Put you on rev 2. Comple 3. Attach mail 4. Use uninform 5. Do not for 6 t DTIC: 1. Assign 2. Return 20000717 044
A. ORIGINATING AGENCY NAVAL POSTGRADUATE SCHOOL, MONTEREY, CA 93943		
B. REPORT TITLE AND/OR NUMBER Changing Mass Applications in An Advanced Time Domain Ship Motion Program.		
C. MONITOR REPORT NUMBER BY: Paul R. Wynn, Thesis, MIT, June 2000		
D. PREPARED UNDER CONTRACT NUMBER N62271-97-G-0026		
2. DISTRIBUTION STATEMENT APPROVED FOR PUBLIC RELEASE; DISTRIBUTION UNLIMITED		

DTIC Form 50
DEC 91

PREVIOUS EDITIONS ARE OBSOLETE

Changing Mass Applications in an Advanced Time Domain Ship Motion Program

by

Paul Richard Wynn

Submitted to the Department of Ocean Engineering
on 22 May 2000, in partial fulfillment of the
requirements for the degree of
Naval Engineer

Abstract

Models are developed for a state-of-the-art time-domain ship motion program to predict ship motions during flooding and green water on deck events. Water mass from the flooding and green water is incorporated into the dynamic equations of motion using time-dependent mass and moment of inertia terms.

Green water on deck includes three subproblems: the problem of water shipping on deck, the problem of motion of water trapped on the deck, and the problem of water escaping off the deck. This research looks at the first two subproblems, both of which involve shallow water wave theory. Glimms method, also called the Random Choice Method, and the Flux Difference Splitting Method are both investigated as solution techniques for the motion of water on deck.

This work provides a tool to estimate ship damaged stability and examine the effects of progressive flooding.

Thesis Supervisor: Dick K.P. Yue

Title: Professor of Hydrodynamics and Ocean Engineering

Contents

1	Introduction	8
1.1	Background	8
1.2	Research Objectives	10
2	LAMP Description and Development of Equations of Motion	12
2.1	LAMP Description	12
2.2	LAMP Rigid Body Dynamics	17
2.3	LAMP Rigid Body Dynamics With Time-Dependent Mass	19
2.3.1	Infinite Frequency Added Mass and Moment of Inertia	19
2.3.2	Translation:	20
2.3.3	Rotation:	21
2.3.4	Coupled Rotation and Translation Equations:	23
3	Models for Flooding	24
3.1	Compartmentation	24
3.2	Calculations For a Compartment's Flooded Volume	26
3.3	Flooding Simulation	28
3.4	Wind	29
3.5	Causes of Loss of Accuracy in LAMP Flooding Simulations	29
4	Models for the Green Water Problem	31
4.1	Background and Scope of Green Water Model	31
4.2	Flux Difference Splitting Method for Water Motion on Deck	32

4.3	Glimms Method (Random Choice Method) for Water Motion on Deck	36
4.3.1	Solution of the Riemann Problem	37
4.4	Selection of Water Motion on Deck Method	42
4.5	Water Shipping Model	43
4.5.1	Free Surface Elevation for Water Shipping	45
4.5.2	Relative Velocity for Water Shipping	46
4.6	Green Water Model in LAMP	48
5	Validation and Results	52
5.1	Validation	52
5.1.1	Validation of Dynamic Equation of Motion Solver	52
5.1.2	Validation of Compartment Flooded Volume and Moment of Inertia Calculation	53
5.1.3	Validation of Flux Difference Splitting Method	54
5.2	Results for Flooding Models	56
5.2.1	Roll Motion Results	57
5.2.2	Vertical Motion Results	58
5.2.3	Loss of Accuracy Examples	58
5.2.4	Progressive Flooding Results	61
5.3	Results for Green Water	62
6	Conclusions	72
6.1	Discussion and Recommendations	72
6.2	Problems Encountered	73
6.2.1	Computational Difficulties During Rapid Changes in Mass and Mass Distribution	73
6.2.2	Selection of the Time Discretization for the Flux Difference Splitting method	73
6.2.3	Calculating Relative Velocity for the Water Shipping Problem	74
6.3	Recommendations for Future Research	75
A	Moment of Inertia Tensor Calculations	77

B Details of Riemann Problem Calculations	80
C MATLAB Program to Solve Riemann Problem Using the Random Choice Method	94

List of Figures

2-1	Domain Definitions in the LAMP Mixed-Source Formulation	14
2-2	Coordinate Systems for LAMP Dynamic Solver	17
3-1	Compartmentation Model of a DDG51 Class Bow	25
3-2	Compartment Flooded Volume Model	27
4-1	Coordinate System for Two-Dimensional Free Surface	34
4-2	Initial Conditions for the Riemann Problem	38
4-3	Solution for Riemann Problem Case I	39
4-4	Solution for Riemann Problem Case II	40
4-5	Solution for Riemann Problem Case III	41
4-6	Solution for Riemann Problem Case IV	41
4-7	Riemann Problem Solution Using Flux Difference Splitting Method	42
4-8	Riemann Problem Solution Using Random Choice Method	44
4-9	Solution Randomness in Random Choice Method	44
4-10	Geometry and Variables for the Water Shipping Model	45
4-11	Water Shipping	47
4-12	Weatherdeck Division for LAMP Green Water Model	49
4-13	Flow Visualization of Green Water on Deck	51
5-1	Model Used to Validate Dynamic Equations of Motion Solver	52
5-2	Conservation of Linear Momentum	53
5-3	Conservation of Angular Momentum	54
5-4	Bore Propagation at $t = 0.5$ seconds	55

5-5	Shallow Water Sloshing Below Resonant Frequency	56
5-6	Shallow Water Sloshing, Twice Resonance Frequency	57
5-7	Roll Motion Intact and Flooded Ships	59
5-8	Sloshing Effects on Roll Motion	59
5-9	Pitch Motion Intact and Flooded Ships	60
5-10	Heave Motion Intact and Flooded Ship	60
5-11	Flooding Forward, Bow Height Above Free Surface	63
5-12	Effects of Linear Hydrodynamics and Flooding	63
5-13	Effect of Center of Gravity Shift on Pitch Motion	64
5-14	Progressive Flooding Pitch and Heave Motion	64
5-15	Progressive Flooding Relative Bow Height	65
5-16	Linear and Nonlinear Progressive Flooding Pitch Motion Calculation	65
5-17	Linear and Nonlinear Progressive Flooding Relative Bow Height Calculation	68
5-18	Effects of Green Water on Pitch Motion	68
5-19	Effects of Green Water on Heave Motion	69
5-20	Relative Bow Height and Green Water Mass on Deck	69
5-21	Mass on Deck Using Different Shipping Water Velocities	70
5-22	Green Water Mass on Deck and Mass Center	70
5-23	Pitch Motion and Local Green Water Deck Loads	71
A-1	Parallelepiped	77
A-2	Rotation of Coordinate Systems	79
B-1	Initial Conditions for the Riemann Problem	81
B-2	Initial Conditions for Riemann Problem in Steady Velocity Frame	82
B-3	Advancing Bore	83
B-4	Case I, Coordinate System Translating at V_0	85
B-5	Case II, Fixed Coordinate System	87
B-6	Case III, Fixed Coordinate System	89
B-7	Case IV, Fixed Coordinate System	91
B-8	Case V, Fixed Coordinate System	93

Chapter 1

Introduction

1.1 Background

There are many hazards to ships that can result in hull damage and subsequent flooding. Depending on the extent of a ship's damaged condition, flooding may cause a loss of buoyancy, a loss of transverse stability, and significant changes in trim and list. Adverse buoyancy and trim conditions can lead to sinking by foundering, while the loss of transverse stability can lead to capsizing. Significant trim and list changes may also result in water on the weatherdeck due to shipping water as freeboard is lost. The water on deck, often referred to as green water or the green water problem, can further harm a damaged ship's stability condition and also affect the main hull girder loads, and deck and superstructure loads.

The state of stability, list, and trim in a damaged ship is dynamic; it varies over time as the flooding event progresses and also depends strongly on environmental conditions such as sea state and wind. Current naval standards, however, take a static approach in specifying stability requirements for a damaged ship. For example, the naval standard DDS-079, reference [5], requires that stability be analyzed on the equilibrium position of the damaged ship based purely on static geometry after the flooding event is complete. This analysis is similar in many respects to intact stability calculations except with characteristics such as metacenter, center of gravity, and righting arm curves adjusted due to the weight of water in the flooded compartments. Reference [5] makes use of wind speed and wave height for damaged stability analysis, but these environmental conditions are also applied to the analysis in a static sense

through applying steady wind heeling moments and placing limitations on bulkhead opening locations. Reference [9] refers to such bulkhead locations as "V-lines."

In [31] Surko points out limitations due to the static approach of current damaged stability analysis procedure and criteria. Of these limitations, two are becoming more salient as the US Navy shifts to performance based requirements. First, in 1987 the Chief of Naval Operations (CNO) [24] endorsed a series of operational characteristics to be incorporated into surface combatants of the year 2010. Included in these characteristics is that a ship has the capability to fight, even though it may have sustained hull damage and be flooded, with whatever weapons systems are available. To assess whether a ship could employ weapons while fighting hurt would require analyzing ship motions which is well beyond the scope of reference [5] procedures. In fact references [14], [15], and [16] report there is no information in the literature and no appropriate computer prediction tools to assess ship motion performance of partially flooded or flooding ships in waves and wind. The second significant limitation in current damaged stability criteria pointed out by Surko is that moderate wind and sea conditions are assumed. In reference [31] Surko shows there is a considerable probability of experiencing wave action that exceeds the moderate 8 foot wave height assumed in reference [5].

As a first step in addressing these limitations, model tests have been performed to assess the dynamic stability of current fleet combatants in a damaged condition. These tests were reported in references [14], [15], and [16]. The term "dynamic stability" in these model tests is meant in its true sense: actual ship motions and ability to withstand sinking under a variety of environmental and flooding conditions.

Model testing can be costly due to production of scale models and the use of large laboratory facilities for the experiments. Also, the time requirements to prepare and conduct model tests make it difficult to use testing early in the design process to predict damaged dynamic stability for immature designs and design variants. Development of damaged stability computer prediction tools, especially for early in the design process, would be ideal as a supplement or replacement to model testing.

Computational fluid dynamic (CFD) codes that predict ship motion would provide a good foundation for development of damaged stability prediction tools. Of the two general categories of CFD codes that predict ship motion, frequency domain and time domain, the time domain

approach is better suited for damaged stability analysis. Frequency domain codes only consider the mean underwater hull form and linearize by assuming small wave and motion amplitudes. The linear prediction would breakdown under high sea states and large amplitude responses that need to be considered for a damaged stability analysis. On the other hand, state of the art CFD codes that predict wave-induced ship motions and loads in the time domain solve the non-linear three-dimensional ship motion problem and can handle large wave and motion amplitudes.

Also, inherent in use of a time domain code as a damage stability prediction tool is the ability to predict motions during the entire flooding event. Such a tool would be useful at assessing the effects of progressive flooding. Progressive flooding occurs when water in flooded compartments floods into adjacent compartments by overflowing watertight bulkheads or leaking through damaged bulkheads. The R.M.S. Titanic sank as a result of progressive flooding which flooded compartments beyond those originally opened to the sea by the iceberg-caused damage. Progressive flooding is of special concern in warships where hull damage from combat is likely to cause the watertight bulkheads surrounding the affected compartments to suffer some damage from shock or fragmentation. The US Navy has an interest in progressive flooding but the published work to date, an example of which is in reference [2], has been simple quasistatic models that do little more than determine the damaged ship hydrostatic position throughout the progressive flooding event.

1.2 Research Objectives

This research investigates the addition of a compartment flooding model and green water model to a CFD code that predicts ship motions in the time domain so that it can be used as a damaged stability prediction tool. There is no effort made by the author to perform damaged stability analysis. The specific CFD code used for these purposes is the Large Amplitude Motions Program (LAMP) developed by the Ship Technology Division of Science Application International Corporation (SAIC). The theory and some results of the LAMP code have been presented in several papers including references [7], [26], and [19]. A brief review of the theory and formulations of LAMP is given in Chapter 2.

Green water and compartment flooding can be considered as events that, at each instant, are part of the ship and change the total rigid body mass and mass distribution. Sloshing and water motion will also affect the mass distribution. Both events are fundamentally the same process that can be modeled as a time-rate-of-change of ship mass in the rigid body motion problem. The approach in this thesis, then, is to calculate the affect on ship motions from green water and flooding by incorporating time-dependent mass and mass moment of inertia into the LAMP dynamic equations of motion solver.

The green water problem includes three subproblems: water shipping; motion of water on deck; and water escaping off deck. This research looks at the first two subproblems in some detail. Water escaping is treated by simply letting water fall off the weatherdeck edges.

The water motion on deck subproblem involves shallow water wave theory. There are several solution techniques that have been developed to solve the shallow water wave problem. Two of the techniques, Glimms method (also called the Random Choice Method) and the Flux Difference Splitting Method, are robust in the sense that they can handle dicontinuities such as shocks and bores in the solution. This research investigates implementation of both solution techniques. As a result, the flux difference splitting method is selected as the solution technique for shallow water flow in the green water model.⁶

Chapter 2

LAMP Description and Development of Equations of Motion

2.1 LAMP Description

This description of LAMP is primarily based on information from reference [21]. LAMP computes a time domain solution for a general three-dimensional body floating on a free surface. Six degree-of-freedom motions are permitted. LAMP obtains a potential flow solution to the body-wave interaction problem using the boundary-element (or panel) method where the submerged body surface is divided into a number of panels. The incoming waves can take any form. At each time step the hydrodynamic pressure forces on the hull, which are computed from the complete velocity potential solution, are combined with body forces and any external forces to solve the equations of motion. The hull pressure forces may also be used to calculate hull bending and torsional moments and shear forces.

In order to balance computation requirements with physics correctness and complexity, LAMP has three methods of calculation. The user selects a specific calculation method for a LAMP run through control variables specified in the input. The LAMP calculation methods are compared in Table 2.1.

Method	Hydrodynamic, Restoring, and Froude-Krylov Wave Forces
LAMP-1	Free Surface Boundary Condition on Mean Water Surface 3-D Linear Hydrodynamics Linear Hydrostatic Restoring and Froude-Krylov Wave Forces
LAMP-2	Free Surface Boundary Condition on Mean Water Surface 3-D Linear Hydrodynamics Nonlinear Hydrostatic Restoring and Froude-Krylov Wave Forces
LAMP-4	Free Surface Boundary Condition on Incident Water Surface 3-D Nonlinear Hydrodynamics Nonlinear Hydrostatic Restoring and Froude-Krylov Wave Forces

Table 2.1: LAMP Calculation Methods and Description

The LAMP-4 method is the complete large-amplitude method where the 3-D velocity potential is computed with the linearized free-surface condition satisfied on the surface of the incident wave. Both the hydrodynamic and hydrostatic pressure are computed over the instantaneous hull surface below the incident wave surface. The incoming wave slope must be small. Small slope generally indicates that the wave height is one order of magnitude less than the wavelength. LAMP-4 has large computational requirements and has traditionally been run on a supercomputer. However, the mixed-source formulation now used in LAMP to solve the potential flow problem provides enough computational savings for LAMP-4 to be run on a workstation. The mixed source formulation is discussed later in this chapter.

The LAMP-2 method is an approximate nonlinear method which retains many of the advantages of both LAMP-1 and LAMP-4. It uses a linear 3-D approach like LAMP-1, where the potential flow problem is solved over the mean body boundary position, to compute the hydrodynamic (radiation, diffraction, and forward speed) part of the pressure forces. The hydrostatic restoring and Froude-Krylov wave forces are calculated on the portion of the ship beneath the incident wave surface. The requirements for computer resources are about the same as LAMP-1. Note that the LAMP-2 and LAMP-4 nonlinear methods are based on the approach that both the ship motions and the waves may have large amplitudes.

The LAMP-1 method is the linearized version of the LAMP-4 method with the free surface boundary conditions satisfied on the undisturbed free surface location. The linear hydrostatic

restoring forces are computed from waterplane quantities while the Froude-Krylov wave forces are calculated with pressure below the undisturbed free surface location. Like LAMP-2, the mean body boundary position is used for the potential flow problem.

LAMP uses two approaches toward solving the hydrodynamic problem for the potential function $\Phi(t)$ at each time step: a direct solution of the hydrodynamic potentials in the time domain and a solution using pre-computed impulse response functions. Both solutions are based upon a mixed-source formulation that is briefly described in the remainder of this section.

In the mixed-source formulation, both the Rankine source and the transient Green function are used. The fluid domain is divided into an inner domain *I* and an outer domain *II* as shown in figure 2-1. The inner domain is enclosed by the wetted body surface S_b , a local portion of the free surface S_f , and the matching surface S_m . The free surface S_f intersects the body surface and is truncated by the matching surface S_m at the water line Γ_m . The outer domain is the rest of the fluid region enclosed by S_m , an imaginary surface S_∞ , and the remaining free surface intersected by S_m and S_∞ .

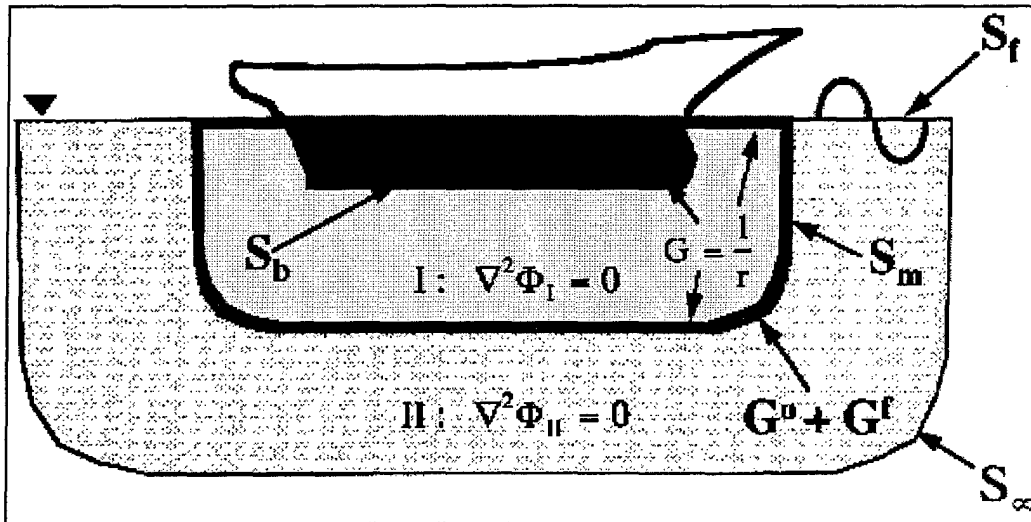


Figure 2-1: Domain Definitions in the LAMP Mixed-Source Formulation

The fluid motion is described by a velocity potential,

$$\Phi_T(\vec{x}, t) = \Phi_W(\vec{x}, t) + \Phi(\vec{x}, t) \quad (2.1)$$

where Φ_W is the incident wave potential and Φ is the total disturbance potential due to the presence of the ship. \vec{x} is a position vector and t is time. In the inner domain I , the initial boundary value problem for $\Phi = \Phi_I$ can be expressed as,

$$\nabla^2 \Phi_I = 0 \quad \text{in } I \quad (2.2)$$

The inner domain potential must satisfy the free surface and body boundary conditions. The free surface boundary condition is linearized in all three formulations, such that

$$\frac{\partial^2 \Phi_I}{\partial t^2} + g \frac{\partial \Phi_I}{\partial z} = 0 \quad \text{on } S_f(t), t > 0 \quad (2.3)$$

where g is the gravitational acceleration. The body boundary condition is next applied on the instantaneous underwater body for LAMP-4 and the mean underwater body for LAMP-1 and LAMP-2,

$$\frac{\partial \Phi_I}{\partial \vec{n}} = \vec{V}_n - \frac{\partial \Phi_W}{\partial \vec{n}} \quad \text{on } S_b(t), t > 0 \quad (2.4)$$

where \vec{n} is a unit normal vector to the body out of the fluid and \vec{V}_n is the instantaneous body velocity in the normal direction. $S_b(t)$ is constant for LAMP-1 and LAMP-2. Finally, the initial conditions require a zero disturbance potential on the free surface at $t = 0$,

$$\Phi_I = \frac{\partial \Phi_I}{\partial t} = 0 \quad \text{at } t = 0 \quad (2.5)$$

The corresponding boundary integral equation in terms of the Rankine source is,

$$2\pi \Phi_I(P) + \int_{S_I} (\Phi_I G_n - \Phi_{In} G) dS = 0 \quad (2.6)$$

where $G = 1/r = 1/|P - Q|$. $P = (x, y, z)$ and $Q = (\xi, \eta, \zeta)$ are the field point and source point on $S_I = S_f \cup S_b \cup S_m$.

In the outer domain II , the initial-value boundary problem for $\Phi = \Phi_{II}$ can be written as,

$$\nabla^2 \Phi_{II} = 0 \quad \text{in } II \quad (2.7)$$

$$\frac{\partial^2 \Phi_{II}}{\partial t^2} + g \frac{\partial \Phi_{II}}{\partial z} = 0 \quad \text{on } S_f(t), t > 0 \quad (2.8)$$

$$\begin{aligned} \nabla\Phi_{II} &\rightarrow 0 && \text{at } \infty \\ \Phi_{II} = \frac{\partial\Phi_{II}}{\partial t} &= 0 && \text{at } t = 0 \end{aligned} \quad (2.9)$$

The corresponding boundary integral equation in terms of the Rankine source is,

$$2\pi\Phi_{II}(P) + \int_{S_m} (\Phi_{II}G_n^o - \Phi_{II_n}G^o)dS = M(P, t) \quad (2.10)$$

where the memory function $M(P, t)$ is defined as,

$$M(P, t) = \int_0^t d\tau \left\{ \int_{S_m} (\Phi_{II}G_{\tau n}^f - \Phi_{II_n}G_{\tau}^f)dS + \frac{1}{g} \int_{\Gamma_m} (\Phi_{II}G_{\tau\tau}^f - \Phi_{II\tau}G_{\tau}^f)V_N dL \right\} \quad (2.11)$$

where Γ_m is the water line of the matching surface, V_N is the normal velocity of Γ_m , and G^o and G^f are associated with the transient Green function. Reference [29] provides a detailed description of the transient Green function.

The matching surface is treated as a control surface and moves with the body. To complete the problem statement, the matching conditions require that the total disturbance velocity potential and the normal velocity across the matching surface are continuous, thereby producing

$$\Phi_I = \Phi_{II} \quad \text{on } S_m \quad (2.12)$$

$$\frac{\partial\Phi_I}{\partial n} = \frac{\partial\Phi_{II}}{\partial n} \quad \text{on } S_m \quad (2.13)$$

The solution is obtained at each time step. Using the panel method, the above equations are used to solve for Φ_I on S_b , $\frac{\partial\Phi_I}{\partial n}$ on S_f , and Φ_I and $\frac{\partial\Phi_I}{\partial n}$ on S_m . Bernoulli's equation is used to compute the pressure on the hull surface, which is integrated to get the hydrodynamic forces on the ship. Then the linearized free surface boundary condition can be used in domain I to integrate in time and update the values of the total disturbance wave elevation and Φ_I at the next time step.

2.2 LAMP Rigid Body Dynamics

This section outlines the solution in LAMP to the rigid body dynamic problem. Several coordinate systems, illustrated in figure 2-2, are used to describe the six-degree-of-freedom motion of a ship in a seaway. The global system, \mathbf{Og} , is fixed on earth. A second system is the local system, \mathbf{O}' , which is fixed at the ship's center of mass, \mathbf{cg} , and rotates with the ship. The relation between these two systems is by the position vector, $\vec{\mathbf{R}}$, and a set of euler angles, $\vec{\Omega} = (\Phi_r, \Theta, \Psi)$, measured in the global system and following the sequence of rotation Ψ , Θ , and Φ_r , respectively, from \mathbf{Og} to \mathbf{O}' . The angles $\vec{\Omega}$ can be thought of in common terms: Ψ is

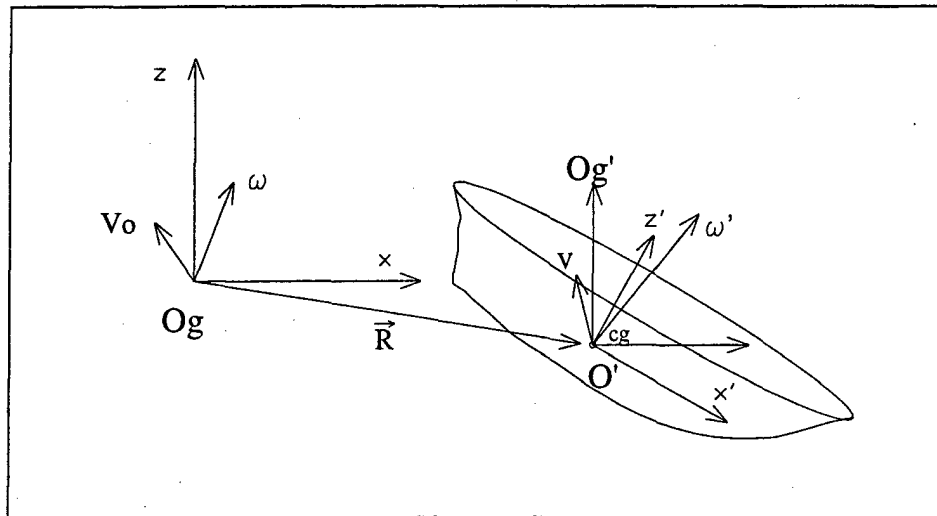


Figure 2-2: Coordinate Systems for LAMP Dynamic Solver

the ship's yaw, Θ is the ship's pitch, and Φ_r is the ship's roll. The matrix $\bar{\mathbf{L}}$ is the euler angle transformation matrix between \mathbf{Og} and \mathbf{O}' .

$$\bar{\mathbf{L}} = \begin{bmatrix} \cos \Psi \cos \Theta & \sin \Psi \cos \Theta & -\sin \Theta \\ -\sin \Psi \cos \Phi_r + \cos \Psi \sin \Theta \sin \Phi_r & \cos \Psi \cos \Phi_r + \sin \Psi \sin \Theta \sin \Phi_r & \cos \Theta \sin \Phi_r \\ \sin \Psi \sin \Phi_r + \cos \Psi \sin \Theta \cos \Phi_r & -\cos \Psi \sin \Phi_r + \sin \Psi \sin \Theta \cos \Phi_r & \cos \Theta \cos \Phi_r \end{bmatrix} \quad (2.14)$$

A third coordinate system, \mathbf{Og}' , has the same orientation as \mathbf{Og} but is initially centered at \mathbf{cg} and moves with steady ship speed, U_{ship} . There are other coordinate systems used in LAMP

to define the rigid body geometry, for example the input and initial static systems, but these are not necessary in describing the solution to the dynamic equations of motion.

Velocities for the dynamic problem are defined as follows. All linear velocities are referred to the global coordinate system unless indicated. \vec{V}_O is the velocity of a point on the rigid body, or extended rigid body, that coincides with Og at time t ; \vec{V} is the rigid body velocity at cg ; \vec{V}_g is the rigid body velocity at cg referred to the O'_g system. $\vec{\omega}$ is the absolute angular velocity and $\vec{\omega}'$ is the angular velocity in local system, O' .

The velocities are related by

$$\vec{V} = \vec{V}_O + \vec{\omega} \times \vec{R} \quad (2.15)$$

$$\vec{V} = \frac{d}{dt} \vec{R} \quad (2.16)$$

$$\vec{V}_g = \vec{V}_O - U_{ship} \quad (2.17)$$

$$\vec{\omega}' = \bar{L} \vec{\omega} \quad (2.18)$$

$$\vec{\omega} = \bar{L}^T \vec{\omega}' \quad \text{and} \quad \frac{d}{dt} \vec{\omega} = \bar{L}^T \frac{d}{dt} \vec{\omega}' \quad (2.19)$$

The rate of change of $\vec{\Omega}$ in terms of the angular velocity of the ship, $\vec{\omega}'$, is given by

$$\frac{d}{dt} \vec{\Omega} = [W] \vec{\omega}' \quad (2.20)$$

where $[W]$ is defined as

$$[W] = \begin{bmatrix} 1 & \sin \Phi_r \sin \Theta / \cos \Theta & \cos \Phi_r \sin \Theta / \cos \Theta \\ 0 & \cos \Phi_r & -\sin \Phi_r \\ 0 & \sin \Phi_r / \cos \Theta & \cos \Phi_r / \cos \Theta \end{bmatrix} \quad (2.21)$$

To determine \vec{R} and $\vec{\Omega}$ the dynamic equations for the rigid body motion must be solved. The equation of motion for translation can be written as

$$\vec{F}_O = \frac{d}{dt} ((\bar{M}o)(\vec{V}_O - U_{ship})) \quad (2.22)$$

where \vec{F}_O is the total force acting on the rigid body at cg and $\bar{M}o$ is the rigid body mass matrix.

The equation of motion for rotation about \mathbf{cg} in the local coordinate system can be written as

$$\overline{\mathbf{M}}\dot{\boldsymbol{\omega}} = \overline{\mathbf{L}}^T \overline{\mathbf{I}} \frac{d}{dt}(\overline{\boldsymbol{\omega}}') + \overline{\mathbf{L}}^T (\overline{\boldsymbol{\omega}}' \times \overline{\mathbf{I}} \overline{\boldsymbol{\omega}}') \quad (2.23)$$

where $\overline{\mathbf{M}}\dot{\boldsymbol{\omega}}$ is the total moment acting on the rigid body about \mathbf{cg} in the \mathbf{Og} or \mathbf{Og}' coordinate system and $\overline{\mathbf{I}}$ is the rigid body mass moment of inertia tensor in the local coordinate system. $\overline{\mathbf{F}}_0$ and $\overline{\mathbf{M}}\dot{\boldsymbol{\omega}}$ are calculated from the instantaneous total force including hydrodynamics and external contributions. Equations 2.22 and 2.23 can be formulated into a coupled system of equations

$$\begin{bmatrix} E \end{bmatrix} \cdot \frac{d}{dt} \begin{bmatrix} \overline{\mathbf{V}}_o \\ \overline{\boldsymbol{\omega}}' \end{bmatrix} = \begin{bmatrix} q \end{bmatrix} \quad (2.24)$$

Combining equations 2.24, 2.16, and 2.20 yields

$$\frac{d}{dt} \begin{bmatrix} \overline{\mathbf{V}}_o \\ \overline{\boldsymbol{\omega}}' \\ \overline{\mathbf{R}} \\ \overline{\boldsymbol{\Omega}} \end{bmatrix} = \begin{bmatrix} \begin{bmatrix} E \end{bmatrix}^{-1} \begin{bmatrix} q \end{bmatrix} \\ \overline{\mathbf{V}} \\ [W] \overline{\boldsymbol{\omega}}' \end{bmatrix} \quad (2.25)$$

Equation 2.25 is solved by the fourth order Runge-Kutta method.

2.3 LAMP Rigid Body Dynamics With Time-Dependent Mass

The solution to the rigid body dynamic problem requires some modification to account for time-dependent mass and mass moment of inertia tensor due to water added to a ship from flooding or shipping water. Also, water motion will change the mass moment of inertia tensor over time. This section provides a detailed formulation of the rigid body dynamics solution with time-dependent mass and mass moment of inertia tensor.

2.3.1 Infinite Frequency Added Mass and Moment of Inertia

The solution to the rigid body dynamic equations of motion in LAMP makes use of the ship's infinite frequency added mass and moment of inertia. This section defines these terms and

explains why they are used.

LAMP calculates the total instantaneous force, \vec{F}_o , and moment, \vec{M}_o , for the ship rigid body dynamic equations. Force and moment contributions from hydrostatics, the incident wave, hydrodynamics, external forces, and body forces are used to calculate \vec{F}_o and \vec{M}_o . Due to the total nature of the force and moment calculation the infinite frequency added mass and moment of inertia for the ship are not required in the dynamic equations. However, they are used in the LAMP rigid body dynamic solution for numerical stability.

The added mass and added moment of inertia terms are referred to the global coordinate system when calculated. This causes them to be time-varying as the rigid body orientation changes with respect to the global system. The added mass and added moment of inertia terms are defined at an each time instant as

$$a_{ij} = \rho \iint_B \phi_i \frac{\partial \phi_j}{\partial n} dS \quad i, j = 1, 2, \dots, 6 \quad (2.26)$$

where $\frac{\partial \phi_i}{\partial n} = n_i$, $i = 1, 2, 3$ and $\frac{\partial \phi_i}{\partial n} = (\vec{r}_s \times \vec{n})_{i-3}$, $i = 4, 5, 6$. Vector \vec{r}_s is the position vector on the body, B , in the local coordinate system and \vec{n} the outward normal of the fluid on B . The global added mass matrix, \overline{A}_o , is a 6x6 matrix constructed with term i, j of \overline{A}_o equal to a_{ij} . The terms in \overline{A}_o are defined as 3x3 submatrices

$$\overline{A}_o = \begin{bmatrix} \overline{A}_{110} & \overline{A}_{120} \\ \overline{A}_{210} & \overline{A}_{220} \end{bmatrix} \quad (2.27)$$

2.3.2 Translation:

By replacing the rigid body mass matrix, \overline{M}_o , with $\overline{M}_o + \overline{\Delta m}(t)$, the equation of motion for translation can be written as,

$$\vec{F}_o = \frac{d}{dt}((\overline{M}_o + \overline{\Delta m}(t))(\vec{V}_o - U_{ship})) \quad (2.28)$$

For stability in the Runge-Kutta numerical integration scheme, added mass terms are added to both sides of equation 2.28 to obtain

$$\vec{\mathbf{F}}_0 + \overline{A_{110}} \frac{d}{dt}(\vec{\mathbf{V}}_o) + \overline{A_{120}} \frac{d}{dt}(\vec{\boldsymbol{\omega}}) = \frac{d}{dt}((\overline{M}_o + \overline{\Delta m}(t))(\vec{\mathbf{V}}_o - Uship)) + \overline{A_{110}} \frac{d}{dt}(\vec{\mathbf{V}}_o) + \overline{A_{120}} \frac{d}{dt}(\vec{\boldsymbol{\omega}}) \quad (2.29)$$

Rewrite equation 2.29 by substituting $\vec{\mathbf{F}}$ for the left hand side where $\vec{\mathbf{F}} = \vec{\mathbf{F}}_0 + \overline{A_{110}} \frac{d}{dt}(\vec{\mathbf{V}}_o) + \overline{A_{120}} \frac{d}{dt}(\vec{\boldsymbol{\omega}})$

$$\vec{\mathbf{F}} = \frac{d}{dt}((\overline{M}_o + \overline{\Delta m}(t))(\vec{\mathbf{V}}_o - Uship)) + \overline{A_{110}} \frac{d}{dt}(\vec{\mathbf{V}}_o) + \overline{A_{120}} \frac{d}{dt}(\vec{\boldsymbol{\omega}}) \quad (2.30)$$

then group terms and carry out differentiation to get the final form of the translation equation of motion

$$\vec{\mathbf{F}} = (\overline{M}_o + \overline{\Delta m}(t) + \overline{A_{110}}) \frac{d}{dt}(\vec{\mathbf{V}}_o) + \overline{A_{120}} \overline{L}^T \frac{d}{dt}(\vec{\boldsymbol{\omega}}) + (\vec{\mathbf{V}}_o - Uship) \frac{d}{dt}(\overline{\Delta m}(t)) \quad (2.31)$$

2.3.3 Rotation:

The rotation equation of motion is expressed in the local frame \mathbf{O}' . The local frame is used so that derivatives of $\overline{\mathbf{I}}$ and $\overline{\mathbf{L}}$ do not have to be calculated.

Definitions and relations:

Some terms need definition prior to developing the rotation equation of motion. $\overline{\mathbf{I}}$ is the rigid body mass moment of inertia tensor in the \mathbf{O}_g or \mathbf{O}_g' frame. $\overline{\mathbf{H}}$ is the angular momentum about \mathbf{cg} in the \mathbf{O}_g or \mathbf{O}_g' frame. $\overline{\mathbf{H}}'$ is the angular momentum about \mathbf{cg} in the \mathbf{O}' frame.

The following equations relate the rotational terms:

$$\overline{\mathbf{H}} = \overline{\mathbf{I}} \vec{\boldsymbol{\omega}} \quad (2.32)$$

$$\overline{\mathbf{H}}' = \overline{\mathbf{I}}' \vec{\boldsymbol{\omega}}' \quad (2.33)$$

$$\overline{\mathbf{M}}_{o'} = \overline{\mathbf{L}} \overline{\mathbf{M}}_o \quad (2.34)$$

$$\overline{\mathbf{I}} = \overline{\mathbf{L}}^T \overline{\mathbf{I}}' \overline{\mathbf{L}} \quad (2.35)$$

Formulation:

The equation of motion for rotation about \mathbf{cg} in the \mathbf{O}' coordinate system can be written as,

$$\vec{\mathbf{M}}_{\mathbf{O}'} = \frac{d}{dt}(\vec{\mathbf{H}}') \quad (2.36)$$

In order to expand the term $\frac{d}{dt}(\vec{\mathbf{H}}')$, the following equation, which is a standard result from any dynamics textbook for vector derivatives in rotating systems, is used,

$$\frac{d}{dt}(\vec{\mathbf{A}}) = \frac{d}{dt}(\vec{\mathbf{A}})_r + \vec{\omega} \times \vec{\mathbf{A}} \quad (2.37)$$

In equation 2.37, $\frac{d}{dt}(\vec{\mathbf{A}})$ is the absolute rate of change of $\vec{\mathbf{A}}$ written terms of the unit vectors in the rotating system, $\frac{d}{dt}(\vec{\mathbf{A}})_r$ is the rate of change of $\vec{\mathbf{A}}$ as viewed from the rotating system, and $\vec{\omega}$ is the absolute angular velocity of the rotating system. Placing the angular momentum vector $\vec{\mathbf{H}}'$ into equation 2.37 gives,

$$\frac{d}{dt}(\vec{\mathbf{H}}') = \frac{d}{dt}(\vec{\mathbf{H}}')_r + \vec{\omega}' \times \vec{\mathbf{H}}' \quad (2.38)$$

The angular momentum as viewed from the rotating (local) system is,

$$(\vec{\mathbf{H}}')_r = \bar{\mathbf{I}}' \vec{\omega}' \quad (2.39)$$

inserting equations 2.33, 2.36, and 2.39 into 2.38 gives,

$$\vec{\mathbf{M}}_{\mathbf{O}'} = \frac{d}{dt}(\bar{\mathbf{I}}' \vec{\omega}') + \vec{\omega}' \times \bar{\mathbf{I}}' \vec{\omega}' \quad (2.40)$$

Due to time varying mass, the rigid body mass moment of inertia tensor, $\bar{\mathbf{I}}'$, is replaced by $\bar{\mathbf{I}}_{\mathbf{O}'} + \Delta \bar{\mathbf{I}}'(t)$. Applying equation 2.34 to 2.40 and making the substitution for the time varying inertia results in

$$\vec{\mathbf{L}} \vec{\mathbf{M}}_{\mathbf{O}'} = \frac{d}{dt}((\bar{\mathbf{I}}_{\mathbf{O}'} + \Delta \bar{\mathbf{I}}'(t)) \vec{\omega}') + \vec{\omega}' \times (\bar{\mathbf{I}}_{\mathbf{O}'} + \Delta \bar{\mathbf{I}}'(t)) \vec{\omega}' \quad (2.41)$$

Then, by performing differentiation and moving \bar{L} to the right hand side equation 2.41 becomes

$$\vec{M}_o = \bar{L}^T \left[(\bar{I}_o + \Delta\bar{I}(t)) \frac{d}{dt} \vec{\omega}' + \frac{d}{dt} (\Delta\bar{I}(t)) \vec{\omega}' + \vec{\omega}' \times [(\bar{I}_o + \Delta\bar{I}(t)) \vec{\omega}'] \right] \quad (2.42)$$

Similar to equation 2.29, for stability of the numerical scheme, added mass terms are added to both sides of the equation 2.42. Also, the substitution of $\vec{M} = \vec{M}_o + \overline{A}_{210} \frac{d}{dt} (\vec{V}_o) + \overline{A}_{220} \frac{d}{dt} (\vec{\omega})$ is made so that

$$\vec{M} = \bar{L}^T \left[(\bar{I}_o + \Delta\bar{I}(t)) \frac{d}{dt} \vec{\omega}' + \frac{d}{dt} (\Delta\bar{I}(t)) \vec{\omega}' + \vec{\omega}' \times [(\bar{I}_o + \Delta\bar{I}(t)) \vec{\omega}'] \right] + \overline{A}_{210} \frac{d}{dt} (\vec{V}_o) + \overline{A}_{220} \frac{d}{dt} (\vec{\omega}) \quad (2.43)$$

Finally, grouping terms gives the final form of the rotation equation of motion

$$\vec{M} = \overline{A}_{210} \frac{d}{dt} (\vec{V}_o) + [\overline{A}_{220} \bar{L}^T + \bar{L}^T (\bar{I}_o + \Delta\bar{I}(t))] \frac{d}{dt} \vec{\omega}' + \bar{L}^T \frac{d}{dt} (\Delta\bar{I}(t)) \vec{\omega}' + \bar{L}^T (\vec{\omega}' \times [(\bar{I}_o + \Delta\bar{I}(t)) \vec{\omega}']) \quad (2.44)$$

2.3.4 Coupled Rotation and Translation Equations:

The translational and rotational equations of motion, equations 2.31 and 2.44, are a coupled system

$$\begin{bmatrix} E \end{bmatrix} \cdot \frac{d}{dt} \begin{bmatrix} \vec{V}_o \\ \vec{\omega}' \end{bmatrix} = \begin{bmatrix} q \end{bmatrix} \quad (2.45)$$

where

$$\begin{bmatrix} E \end{bmatrix} = \begin{bmatrix} \overline{A}_{110} + \overline{M}_o + \overline{\Delta m}(t) & \overline{A}_{120} \bar{L}^T \\ \overline{A}_{210} & \overline{A}_{220} \bar{L}^T + \bar{L}^T (\bar{I}_o + \Delta\bar{I}(t)) \end{bmatrix} \quad (2.46)$$

and

$$\begin{bmatrix} q \end{bmatrix} = \begin{bmatrix} \vec{F} - (\vec{V}_o - U_{ship}) \frac{d}{dt} (\overline{\Delta m}(t)) \\ \vec{M} - \bar{L}^T (\vec{\omega}' \times (\bar{I}_o + \Delta\bar{I}(t)) \vec{\omega}') - \bar{L}^T \frac{d}{dt} (\Delta\bar{I}(t)) \vec{\omega}' \end{bmatrix} \quad (2.47)$$

The details of $[E]$, and $[q]$ were not shown in equation 2.24. They contain terms similar to equation 2.45 except that there are some new terms in equation 2.45 due to the time-dependent mass and mass moment of inertia. The new terms are $(\vec{V}_o - U_{ship}) \frac{d}{dt} (\overline{\Delta m}(t))$ in the translation equation and $\bar{L}^T \vec{\omega}' \frac{d}{dt} (\Delta\bar{I}(t))$ in the rotation equation. Also, mass and mass moment of inertia vary with time in equation 2.45 but are constant in 2.24.

Chapter 3

Models for Flooding

3.1 Compartmentation

Watertight internal subdivision using bulkheads to form compartments within a ship has been the primary means of limiting the extent of flooding in a damaged ship. During ship design, various bulkhead arrangements are evaluated against operational and damaged stability requirements to determine an optimal ship subdivision. In general, improved damaged stability performance with increased subdivision must be balanced against drawbacks to compartmentation such as weight, interference with arrangements, and access to systems.

The capability to compartmentalize hull geometry had to be added to LAMP in order to model flooding for damaged stability analysis. Since this thesis is concerned with the basic changes necessary to LAMP for it to be used as a damaged stability prediction tool, it was considered adequate that the compartmentation model only use transverse bulkheads. If required for a specific ship configuration or damaged scenario, more detailed compartmentation model with longitudinal bulkheads and damage control decks could be added.

A LAMP program module was written to accept arbitrary transverse bulkhead locations as input. The bulkhead locations are specified by their distance from the ship bow. The distance is normalized through dividing by the overall hull length. Any number of bulkheads can be created. The bulkhead locations are then automatically spliced into the hull geometry description to form compartments that are bounded by forward and aft bulkheads, the hull, and the weatherdeck. Compartments at the bow or stern of the ship use the hull geometry to serve

the place of a forward or aft bulkhead as applicable. Figure 3-1 illustrates compartmentation of the bow of a DDG51 Class hull. In this figure the intersection of each line with other lines

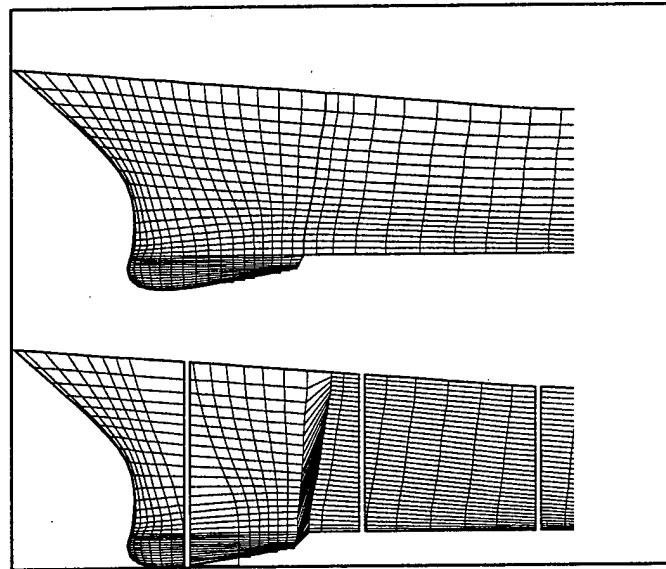


Figure 3-1: Compartmentation Model of a DDG51 Class Bow

is described by an three dimensional coordinate point.

Consistency between the flooded volume calculation and the LAMP hydrostatic calculation is important for an accurate representation of the ship's mean body position. Because the compartmentation module uses the detailed LAMP hull geometry description to define the majority of a compartment, the model provides excellent consistency between the compartment flooded volume calculation and the hydrostatic calculation. Results were obtained for a ship's final hydrostatic position after a flooding event. A comparison of the flooded volume against the resulting change in ship displaced volume showed the two agreed to within 99%.

Finally, the compartmentation module is only used for calculations on the internal flooded water and does not affect the hull geometry description. This is important because the hull geometry description defines the body on which the hydrodynamic calculations are performed.

3.2 Calculations For a Compartment's Flooded Volume

For sloshing of a flooded volume of water it was conservatively assumed the water within a rolling compartment maintains a horizontal surface. In actual ship compartments there are generally some solid objects that will project through the surface of the water to reduce free surface motion. Ship designers account for this effect through the surface-permeability factor.

The horizontal surface assumption produces a first order approximation for sloshing. For simplicity, pitch motion was not considered in the flooded water sloshing calculations. Damaged stability criteria mainly look at transverse stability while in a damaged condition and sloshing due to pitch would have little-to-no effect on this stability. Ignoring pitch motion also made it easier to check the accuracy of the flooded volume calculations.

Numerical solution techniques for calculating the instantaneous dynamic free surface in a flooded compartment are an alternative to assuming a horizontal surface but they provide a relatively small increase in accuracy compared to the significant increase in complexity and calculation time. An actual ship compartment is outfitted and filled with equipment so even if the instantaneous free surface were calculated it probably would not reflect the actual conditions in the flooded compartment. Efforts to accurately calculate a free surface are better suited for the shallow water flow problem that arises when shipping water.

Figure 3-2 illustrates the instantaneous position of a flooded compartment volume with the ship undergoing a roll to starboard with roll angle, Φ_r . The roll is made through the ship's center of gravity, cg . The unprimed coordinate system in the figure, the YZ system, is the LAMP initial static system which is used as the reference to describe the hull and compartment geometry through position vector \vec{R}_{xyz} . The primed coordinate system has been introduced for the flooded volume calculation and rotates to maintain the Y' axis parallel with the water surface.

Flooded compartment volume is calculated in the $Y'Z'$ system by summing the rectangular parallelepipeds of length $del_{y'}$ and height dz' . These are indicated in figure 3-2 and have a depth dx along the hull's longitudinal axis. The parallelepiped geometry was selected to simplify moment of inertia calculation. The flooded volume calculation is initiated by converting the compartment geometry, \vec{R} , to the primed coordinate system, \vec{R}' , where \vec{C} is the rotation matrix

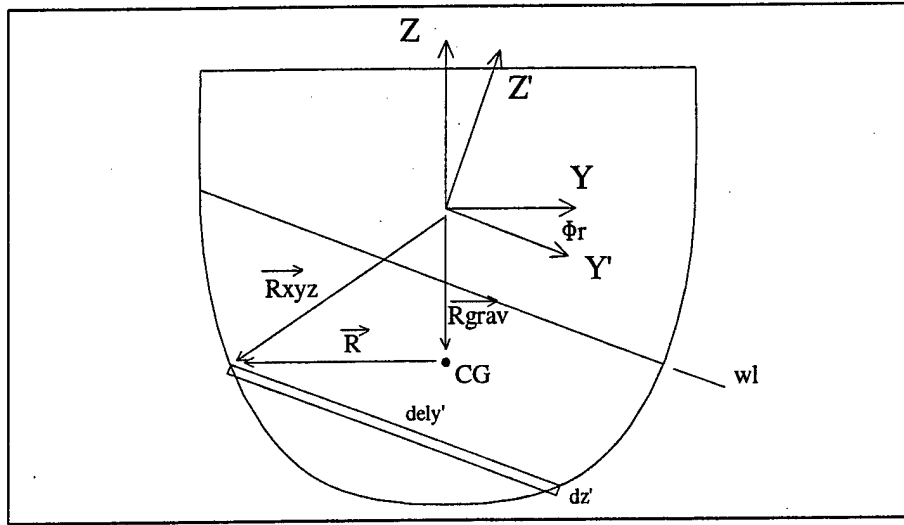


Figure 3-2: Compartment Flooded Volume Model

between YZ and $Y'Z'$,

$$\vec{R}' = \bar{C}(\vec{R}_{xyz} - \vec{R}_{grav}) \quad (3.1)$$

Since only roll motion is considered, the x and x' values are the same. If it were desired to include pitch motion in the sloshing model, the pitch angle could be included in \bar{C} and the calculation proceed in the same manner as described here. The summation for volume is made over x using $j = j_{\max}$ intervals and over z' with $k = k_{\max}$ intervals where x spans the flooded compartment length and z' ranges from the minimum value to the waterline wl

$$V_{cmpt} = \sum_{x_j} \sum_{z'_k} dely'/dz'/dx \quad (3.2)$$

At a fixed roll angle, the waterline value wl serves to determine compartment flooded volume. If a specific instantaneous flooded volume is desired for a particular flooding scenario, wl can be adjusted through an iteration process until the desired volume is reached.

The center of mass of a flooded compartment, $CG_{cmpt} = (x'_1, x'_2, x'_3)$, can be calculated where

$$x'_i = \frac{\sum_{x_j} \sum_{z'_k} x'_i dely'/dz'/dx}{V_{cmpt}} \quad i = 1, 2, 3 \quad (3.3)$$

Equation 3.1 is then used to refer CG_{cmpt} to the YZ coordinate system. With the flooded

volume and center of mass known, forces, moments, and the time-dependent mass terms can be calculated due to the flooded water and added to the dynamic equations of motion 2.45. If the flood rate is specified it is used directly as the $\frac{d}{dt}(\overline{\Delta m}(t))$ term in the equations of motion. Otherwise $\frac{d}{dt}(\overline{\Delta m}(t))$ needs to be calculated based on the flooded volume time history.

The calculation for flooded water mass moment of inertia is made by summing the mass moment of inertia of each parallelepiped about the flooded volume center of mass. Appendix A outlines the method for doing this. After calculating the flooded volume mass moment of inertia tensor about the center of mass, $\overline{SMI}_{c_{mpt}}$, the parallel axis theorem and a rotational transformation must be applied to refer $\overline{SMI}_{c_{mpt}}$ to the ship's cg in the local coordinate system. The instantaneous flooded volume mass moment of inertia tensor is used for the $\Delta \overline{I}(t)$ term in the dynamic equations of motion. The $\frac{d}{dt}(\Delta \overline{I}(t))$ term must be calculated based on the flooded volume mass moment of inertia time history.

To better model an actual ship, compartment permeability could be used in the calculations for a compartment's flooded volume. It would be a trivial matter to add permeability to the calculations above.

3.3 Flooding Simulation

With the compartment flooded volume model established there are several approaches to running a time domain flooding simulation. First, the simulation can start with the initial condition that the flooding event is complete and the ship is in its final flooded static condition. A computer module was written to run this type of simulation. The module solves for a ship's final static position after a flooding event in any specified compartments is complete. The module uses an iterative procedure to calculate the final ship position and then revises the ship mass, moment of inertia tensor, and cg location to account for the added water. Alternatively, the module can maintain the ship intact and provide the total water that would be added if specific compartments were flooded. This information can be used as an upper bound on flooded compartment volume if it is desired to flood the ship as time advances in the simulation.

The second approach for a time domain flooding simulation is to start with either an intact condition or some fully flooded compartments and then flood additional compartments as the

simulation time progresses. This approach is what is referred to as progressive flooding in Chapter 1. The mass addition rate from flooding would need to be specified in this type of simulation. One technique to specify this rate is to specify a hull opening location due to damage and let water enter the compartment when the instantaneous free surface is above the hole. The flow through the hole of area A and at static head h would be governed by the short tube orifice equation, $Q = C_d A \sqrt{2gh}$. Tables may be obtained for the coefficient C_d from textbooks on hydraulics such as LeConte [18]. In [6] Dillingham states C_d may be taken as 0.60 with very good accuracy.

3.4 Wind

LAMP is configured to include external forces in its calculation and currently has modules that calculate external forces for items such as appendages, viscous roll damping, and moving weights. It is a simple matter to include a heeling moment caused by beam winds using an equation such as the following from reference [17]

$$M_W = \frac{K(V_W)^2 A l (\cos(\Phi_r))^2}{\Delta} \quad (3.4)$$

In equation 3.4 V_W is the wind velocity, A is the ship sail area, l is level arm from centroid of sail area to half draft, Φ_r is the roll angle, and Δ is the ship displacement. K is a constant whose value can vary depending on units used in the equation and on assumptions on values for wind drag coefficient. Reference [17] contains a discussion on calculating wind heeling moments. Equation 3.4 could be expanded to include the wind heading angle so that three dimensional wind forces and moments on the ship are included in the LAMP calculation.

3.5 Causes of Loss of Accuracy in LAMP Flooding Simulations

When linear hydrodynamics are used in LAMP to solve the potential flow problem (LAMP-1 and LAMP-2) the initial mean body boundary position is used for the duration of the calculation. However, due to sinkage and trim from flooding the actual mean body boundary position will change. As the flooding ship's mean body position diverges from the initial position a loss of

accuracy in the calculated ship motions will result.

One strategy to limit the loss of accuracy in a flooding simulation using linear hydrodynamics is to select an intermediate body position between the intact and final flooded conditions. Another approach would be to run the linear hydrodynamics LAMP simulation at the intact body position and then at the final flooded body position and use the worse case ship motions as the motion estimate. Of course, non-linear hydrodynamics (LAMP-4) could be used for the flooding simulation but the penalty is that much more time is required to perform the calculation.

As water floods into the ship it causes a time-dependent shift in the ship's center of gravity, cg . This shift is not accounted for in the LAMP dynamic equations of motion solution. For a small amount of flooding in a massive ship the shift in cg will be trivial. Under these conditions the calculated ship motions would be reasonably accurate. However, as the magnitude of the cg shift increases, the calculated angular ship motions will be wrong because the rigid body moment determined at each time step grows in error.

Finally, when simulating significant hull damage such as a compartment size hole, consideration should be given as to whether complete body panelization that assumes an intact hull will provide an accurate enough hydrodynamic solution. A more accurate method may be to re-panelize the hull around the physical damage.

Chapter 4

Models for the Green Water Problem

4.1 Background and Scope of Green Water Model

As a flooding ship loses freeboard, the likelihood of shipping water increases. The water on deck, in turn, can further degrade the ship's stability condition. This is of special concern for smaller vessels. A review paper on the subject of water on deck and stability has been published in reference [3]. Also, in reference [6], Dillingham provides calculations to show that instabilities caused by excessive deck water may cause capsizing of small fishing vessels. The green water problem can be decomposed into three subproblems: shipping water, water escaping off deck, and the motion of water on deck. For adequate modeling of the green water problem in a time domain ship motion program each subproblem must be addressed.

Most work reported on the green water problem has focused on the water motion on deck subproblem. This emphasis over the other two subproblems is primarily due to water-motion-on-deck sharing the same basic theory as that for flow of compressible gases. Specifically, the equations governing water motion on deck, equation 4.13, are derived from the theory for waves in shallow water, covered in detail in reference [29], and are of the same form as the compressible gas dynamics equations. The necessity in industry for dealing with the flow of gases has resulted in numerical solution methods that can be directly applied to the water-motion-on-deck problem. The objective in solving the shallow water equations is to solve for

the water depth and horizontal particle velocity. Solutions to the governing equations can involve discontinuities such as shocks, bores, and hydraulic jumps. Any numerical methods used to solve the equations must be capable of treating discontinuities. Most of the numerical methods fall into two general categories characterized by the scheme used to solve the governing equations: the flux difference splitting method and the random choice method, also known as Glimm's Method. Both schemes handle discontinuities in the solution without any special treatment and were evaluated in this thesis. The Random Choice method involves looking at solution curves, called characteristics, to the governing differential equations. The flux difference splitting method combines a finite difference method with characteristics. A different approach to solving the water on deck problem is in reference [13] where the authors solve for wave motion in a rolling tank using a finite difference scheme coupled with analytical techniques. This approach illustrates the special care that must be taken with discontinuities with which the numerical scheme is incapable of handling.

This chapter develops a green water model for the LAMP program in head seas. The two main methods for solving the water-on-deck subproblem are evaluated for use in the model using a two-dimensional free surface. A method for incorporating water shipping into LAMP is also devised. The water escaping off deck subproblem is not formulated because a proper calculation would require a three-dimensional free surface solution to the shallow-water problem. Three dimensions would introduce transverse water velocities so that as the green water travels aft on the weatherdeck it also moves towards the port and starboard deck edges and then over board. The green water model used for this thesis only calculates longitudinal water velocities so green water mass is removed from the weatherdeck by letting it fall off the after end of the portion of the weather deck included in the computation. This is accomplished by setting boundary conditions for the water-on-deck calculation to zero at the aft end of the weatherdeck

4.2 Flux Difference Splitting Method for Water Motion on Deck

The flux difference splitting method was developed based on the flux vector splitting method originally introduced by Steger and Warming in [28]. Steger and Warming developed a basic theory of the flux vector splitting method to compute the shock wave for the gas dynamic equa-

tions. Because of differences between the non-homogeneous governing equations for shallow water flow on deck and gas dynamics, it is better when solving the shallow water equations to split flux differences instead of the flux vector. In reference [1] Alcrudo presents the flux difference splitting method to solve problems for open channel hydraulics. In references [12] and [11] the flux difference splitting method is applied to solve the shallow water flow on deck problem.

The flux difference splitting method is a an upwind (one-sided) finite difference scheme that solves the shallow water wave propagation problem for a two dimensional free surface. For supercritical flow, wave information can only travel downstream. In the case of subcritical flow, wave information will travel in both directions. In order to construct an upwind scheme valid for all regimes and directions of flow, a decomposition of the flux related to positive and negative propagation speeds is needed. The flux decomposition is devised so that wave information can not travel upstream in supercritical flow. For flux difference splitting methods the flux difference operator, $\Delta \vec{F}$ and $\Delta \overline{RHS}$ in the equations below, is split based on the characteristic directions.

Reference [12] can be used to formulate the shallow water flow governing equations for a two-dimensional free surface with the geometry illustrated in Figure 4-1. Many of the variables in the governing equations are not defined in the figure. Of these, u_1 is the ship surge velocity, u_3 is the ship heave velocity, Θ is the pitch angle, u_5 is the angular velocity, and g is acceleration due to gravity. Note that u is the water particle velocity in the x-direction. The governing equations in vector form is

$$\frac{\partial \vec{W}}{\partial t} + \frac{\partial \vec{F}}{\partial x} = [D] \frac{\partial \vec{H}}{\partial x} + \vec{C} \quad (4.1)$$

where $\vec{W} = \begin{pmatrix} g\zeta \\ ug\zeta \end{pmatrix}$, $\vec{F} = \begin{pmatrix} ug\zeta \\ u^2g\zeta + \frac{1}{2}(g\zeta)^2 \end{pmatrix}$, $\vec{H} = \begin{pmatrix} 0 \\ \frac{1}{2}(g\zeta)^2 \end{pmatrix}$, $[D] = \begin{pmatrix} 0 & 0 \\ 0 & q_1g\zeta + q_2u + q_3 \end{pmatrix}$,

and $\vec{C} = \begin{pmatrix} 0 \\ q_4g\zeta \end{pmatrix}$. The variables q_1 through q_4 are functions of deck motion and geometry.

They are defined as

$$q_1 = \left(\frac{u_5}{g} \right)^2$$

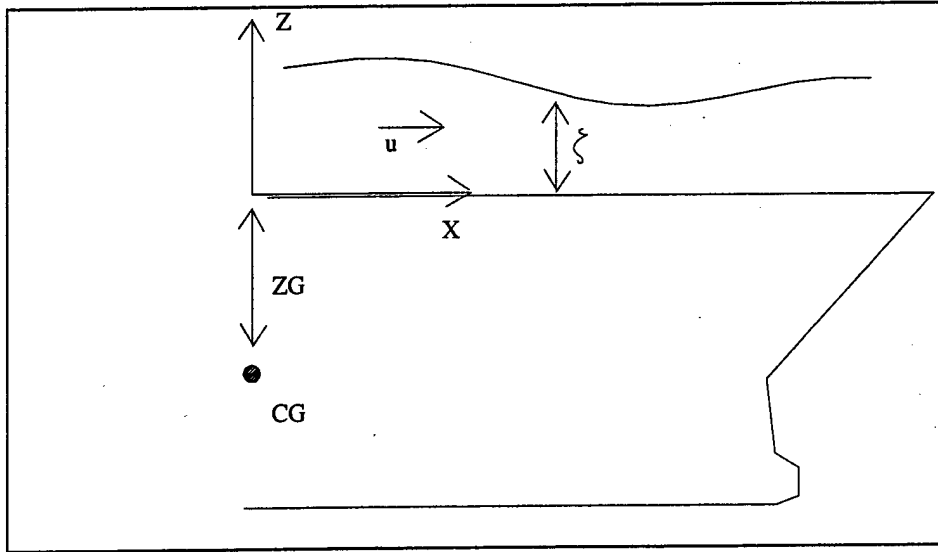


Figure 4-1: Coordinate System for Two-Dimensional Free Surface

$$\begin{aligned}
 q_2 &= 2\frac{u_5}{g} \\
 q_3 &= 1 - \cos(\Theta) - \frac{du_3}{dt} \frac{1}{g} + \frac{du_5}{dt} \frac{x}{g} - \frac{(u_5)^2}{g} \frac{ZG}{g} \\
 q_4 &= g \sin(\Theta) - \frac{du_1}{dt} + (u_5)^2 x + \frac{du_5}{dt} ZG
 \end{aligned}$$

Equation 4.1 is derived by applying the shallow water assumptions to the continuity equation and Eulers equations of motion.

The derivatives of the flux vector \vec{F} and \vec{H} can be expressed in terms of \vec{W}

$$\frac{\partial \vec{F}}{\partial x} = [J_1] \frac{\partial \vec{W}}{\partial x} \quad \text{and} \quad \frac{\partial \vec{H}}{\partial x} = [J_2] \frac{\partial \vec{W}}{\partial x} \quad (4.2)$$

where $[J_1]$ and $[J_2]$ are the Jacobian matrices. The eigenvalues of $[J_1]$ are

$$\lambda_1 = u + \sqrt{g\zeta} \quad \text{and} \quad \lambda_2 = u - \sqrt{g\zeta} \quad (4.3)$$

with the eigenvectors

$$\vec{e}_1 = (1, u + \sqrt{g\zeta})^T \quad \text{and} \quad \vec{e}_2 = (1, u - \sqrt{g\zeta})^T \quad (4.4)$$

The difference of \vec{W} and flux vector \vec{F} are approximated as

$$\Delta \vec{W} = \sum_{k=1}^2 \alpha_k \vec{e}_k \quad \text{and} \quad \Delta \vec{F} = \sum_{k=1}^2 \lambda_k \alpha_k \vec{e}_k \quad (4.5)$$

The right hand side of equation 4.1 equal to zero corresponds to water sloshing for a given initial water surface profile and the ship stationary. With the right hand side zero, the finite difference scheme with the split flux difference can be expressed in the following form

$$\vec{W}_j^{(n+1)} = \vec{W}_j^{(n)} + \frac{\Delta t}{\Delta x} (F_{j-\frac{1}{2}}^* - F_{j+\frac{1}{2}}^*) \quad (4.6)$$

where

$$F_{j+\frac{1}{2}}^* = \frac{1}{2} (\vec{F}_{j+1} + \vec{F}_j) - \frac{1}{2} \sum_{k=1}^2 \alpha_{k,j+\frac{1}{2}} |\lambda_{k,j+\frac{1}{2}}| \vec{e}_{k,j+\frac{1}{2}} \quad (4.7)$$

$$F_{j-\frac{1}{2}}^* = \frac{1}{2} (\vec{F}_j + \vec{F}_{j-1}) - \frac{1}{2} \sum_{k=1}^2 \alpha_{k,j-\frac{1}{2}} |\lambda_{k,j-\frac{1}{2}}| \vec{e}_{k,j-\frac{1}{2}} \quad (4.8)$$

The scheme in equation 4.6 is of the first order.

When the right hand side of equation 4.1 is not equal to zero, it is treated as another flux difference term and projected into the eigenvector space as follows

$$\overline{RHS} = [D] \frac{\partial \vec{H}}{\partial x} + \vec{C} = -\frac{1}{\Delta x} \sum_{k=1}^2 \lambda_k \gamma_k \vec{e}_k \quad (4.9)$$

The right hand side flux difference, where the flux difference is related to equation 4.9 by $\Delta \overline{RHS} = \overline{RHS} \Delta x$, is then split

$$\Delta \overline{RHS}_{j-\frac{1}{2}}^+ = \sum_{k=1}^2 \gamma_{k,j-\frac{1}{2}} \lambda_{k,j-\frac{1}{2}}^+ \vec{e}_{k,j-\frac{1}{2}} \quad \text{and} \quad \Delta \overline{RHS}_{j+\frac{1}{2}}^- = \sum_{k=1}^2 \gamma_{k,j+\frac{1}{2}} \lambda_{k,j+\frac{1}{2}}^- \vec{e}_{k,j+\frac{1}{2}} \quad (4.10)$$

where

$$\lambda_{k,j-\frac{1}{2}}^+ = \frac{1}{2} (\lambda_{k,j-\frac{1}{2}} + |\lambda_{k,j-\frac{1}{2}}|) \quad \text{and} \quad \lambda_{k,j+\frac{1}{2}}^- = \frac{1}{2} (\lambda_{k,j+\frac{1}{2}} - |\lambda_{k,j+\frac{1}{2}}|) \quad (4.11)$$

The split flux difference is then included in the finite difference scheme of equation 4.6

$$\vec{W}_j^{(n+1)} = \vec{W}_j^{(n)} + \frac{\Delta t}{\Delta x} (F_{j-\frac{1}{2}}^* - F_{j+\frac{1}{2}}^*) - \frac{\Delta t}{\Delta x} (\Delta \overline{RHS}_{j-\frac{1}{2}}^+ + \Delta \overline{RHS}_{j+\frac{1}{2}}^-) \quad (4.12)$$

The minus sign in equation 4.12 prior to the \overline{RHS} term is due to the minus sign in equation 4.9. In [28] Steger shows that flux splitting schemes are stable if and only if $|\lambda_k^\pm| \frac{\Delta t}{\Delta x} \leq 1$.

Shallow water first-order schemes suffer from numerical dissipation (the shock front will be smeared). Reference [12] shows how a flux limiter, which is a correction term for the numerical flux, can be applied to the first order scheme to make the scheme higher order.

The flux difference splitting method can be used to solve the shallow water equations for a three-dimensional free surface. Reference [12] formulates a technique using the flux difference splitting method, together with the Fractional Step Method [32], so that solutions to the shallow water equations can be obtained by solving two sets of two-dimensional free surface problems. The three-dimensional solution works as follows. Two sets of vector equations similar to equation 4.1 are devised. One set is for flow in the ship longitudinal direction ($x - axis$) where each specific equation holds for a certain deck strip of thickness Δy . The other set of vector equations is for flow in the transverse direction ($y - axis$) where each equation is for a certain deck strip of thickness Δx . Then the Fractional Step Method advances the solution in time. At each time step the sets of equations along the $x - axis$ are solved for an intermediate solution assuming no y dependency. Then, in the same time step, the sets of equations along the $y - axis$ are solved from the intermediate solution assuming no x dependency. Instead of solving the three-dimensional free surface governing equation on $(m \times n)$ nodes, a total of $(m+n)$ two-dimensional free surface equations are solved along the x and y directions separately using the Fractional Step Method.

The difference schemes of equations 4.6 and 4.12 for a two-dimensional free surface were programmed in a computer so that the method could be compared with Glimms method.

4.3 Glimms Method (Random Choice Method) for Water Motion on Deck

For a two-dimensional free surface, Glimms Method is performed by dividing the physical domain into intervals, $i = 1, 2, 3, \dots, i \text{ max}$. In each interval at time $n\Delta t$ the solution is approximated by piecewise constant depth, ζ_i , and particle velocity, u_i . At the boundary between each interval, the depth and velocity are therefore discontinuous which gives a sequence of Riemann

problems which may be solved to advance the solution to time $(n + 1)\Delta t$. The solution to the Riemann problem is outlined below and the full solution is developed in Appendix B. The Riemann problem is also known as the dam breaking problem. From the time $(n + 1)\Delta t$ Riemann solutions, it is desired to construct another piecewise solution. This is done by randomly sampling the solution in each interval and then using the sampled value as an approximation for that interval's constant piecewise solution. In [10] Glimm showed the random sampling scheme converges to a weak solution. The disturbance resulting from the solution for each individual Riemann Problem must not be able overlap with the disturbance from the adjacent Riemann Problem. No disturbance must be allowed to propagate further than $\frac{\Delta interval}{2}$ in a time Δt . Thus the resulting Courant condition that must be satisfied is $\frac{\Delta interval}{2\Delta t} > (|u| + \sqrt{g\zeta})$. The solution obtained is unconditionally stable.

Glimms Method is used to solve the water motion on deck problem in references [6], [22], and [23]. References [27] and [4] illustrate use of the Glimms Method to solve gas dynamic problems.

Appendix C contains a MATLAB program that solves a Riemann Problem using Glimms Method.

4.3.1 Solution of the Riemann Problem

Glimms method requires solution of the Riemann Problem, also known as the dam breaking problem, at each spatial interval in the computational domain at each time interval. A summary of the Riemann Problem solution procedure, taken from Dillingham [6] follows. Appendix B provides details of the calculations. In keeping with Dillingham's notation, the y axis is used as the coordinate axis for the Riemann Problem, v is the horizontal velocity, and λ is used for the water depth.

The Riemann Problem, illustrated in figure 4-2, consists of solving a system of nonlinear hyperbolic equations, called the shallow water wave equations,

$$\frac{\partial v}{\partial t} + v \frac{\partial v}{\partial y} + g \frac{\partial \lambda}{\partial y} = 0 \quad \text{and} \quad \frac{\partial \lambda}{\partial t} + v \frac{\partial \lambda}{\partial y} + \lambda \frac{\partial v}{\partial y} = 0 \quad (4.13)$$

for a two-dimensional free surface where g is gravity acceleration, subject to initial conditions

on the right-hand and left-hand sides

$$\left. \begin{array}{l} v = V_2 \\ \lambda = \lambda_2 \end{array} \right\} y < 0 \quad \text{and} \quad \left. \begin{array}{l} v = V_0 \\ \lambda = \lambda_0 \end{array} \right\} y > 0 \quad (4.14)$$

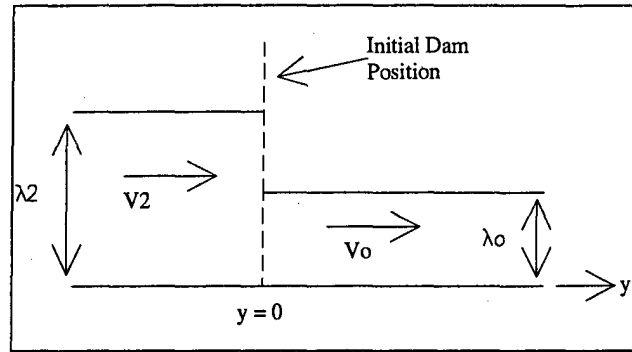


Figure 4-2: Initial Conditions for the Riemann Problem

It is assumed that the water is initially higher on the left side of the dam. The dam is then removed at time $t = 0$. Depending on initial conditions, the Riemann problem solution falls into different categories, identified as Cases I through V. The variable c as used below represents the wave propagation speed; it is the local speed of propagation of "small disturbances" relative to the moving stream. In shallow water theory, c is related to the water height by $c = \sqrt{g\lambda}$.

Solution to the Riemann Problem: Case I

If $V_2 + 2c_2 > V_0 + 2c_0$ and

$$V_2 - V_0 < \left[\frac{g(\lambda_0 + \lambda_1)(\lambda_1 - \lambda_0)^2}{2\lambda_1\lambda_0} \right]^{\frac{1}{2}} \quad (4.15)$$

then the solution consists of a single shock and a single rarefaction as indicated in figure 4-3. Let

$c_0 = \sqrt{g\lambda_0}$, $c_1 = \sqrt{g\lambda_1}$, and $c_2 = \sqrt{g\lambda_2}$. Also, let $R = \frac{\xi - V_0}{c_0}$ where ξ is the shock speed, then

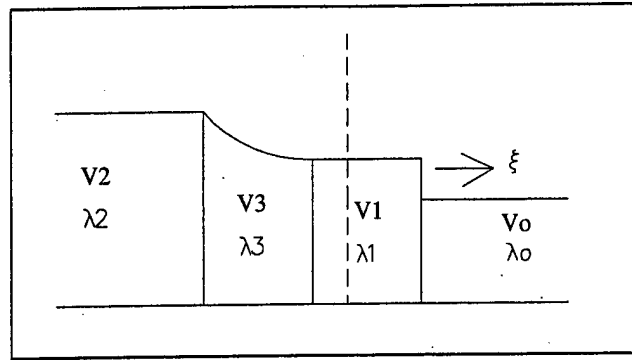


Figure 4-3: Solution for Riemann Problem Case I

solve the following equation for R

$$R - \frac{1}{4R} \left[1 + \sqrt{8R^2 + 1} \right] + 2 \left[\frac{1}{2} \left(\sqrt{8R^2 + 1} - 1 \right) \right]^{\frac{1}{2}} = \frac{V_2 - V_0 + 2c_2}{c_0} \quad (4.16)$$

then we have

$$\xi = c_0 R + V_0 \quad (4.17)$$

$$V_1 = c_0 \left[R - \frac{1}{4R} \left(1 + \sqrt{8R^2 + 1} \right) \right] + V_0 \quad (4.18)$$

$$c_1 = c_0 \left[\frac{1}{2} \left(\sqrt{8R^2 + 1} - 1 \right) \right]^{\frac{1}{2}} \quad \text{and} \quad \lambda_1 = \frac{c_1^2}{g} \quad (4.19)$$

In zone 3 we have

$$v = \frac{2}{3} \left(\frac{y}{t} - V_0 + \frac{V_2 - V_0}{2} + c_2 \right) + V_0 \quad \text{and} \quad \lambda = \frac{1}{9g} \left(V_2 + 2c_2 - \frac{y}{t} \right)^2 \quad (4.20)$$

where zone 3 is bounded by $(V_2 - c_2)t < y < (V_1 - c_1)t$.

Solution to the Riemann Problem: Case II

If equation 4.15 is not satisfied then the solution consists of two shocks as indicated in figure

4-4

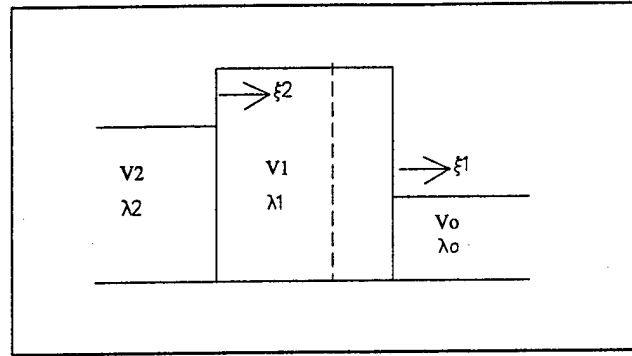


Figure 4-4: Solution for Riemann Problem Case II

Solve the following equation for λ_1

$$V_2 - V_0 - \left[\frac{g(\lambda_0 + \lambda_1)(\lambda_1 - \lambda_0)^2}{2\lambda_1\lambda_0} \right]^{\frac{1}{2}} - \left[\frac{g(\lambda_1 + \lambda_2)(\lambda_2 - \lambda_1)^2}{2\lambda_2\lambda_1} \right]^{\frac{1}{2}} = 0 \quad (4.21)$$

then

$$V_1 = V_0 + \left[\frac{g(\lambda_0 + \lambda_1)(\lambda_1 - \lambda_0)^2}{2\lambda_1\lambda_0} \right]^{\frac{1}{2}} \quad (4.22)$$

$$\xi_1 = \frac{\lambda_1 V_1 - \lambda_0 V_0}{\lambda_1 - \lambda_0} \quad \text{and} \quad \xi_2 = \frac{\lambda_2 V_2 - \lambda_1 V_1}{\lambda_2 - \lambda_1} \quad (4.23)$$

Solution to the Riemann Problem: Case III

If $V_0 - V_2 > 2|c_0 - c_2|$ then the solution consists of two rarefaction waves as in figure 4-5. The solution for zone 1 is

$$V_1 = \frac{V_0 + V_2}{2} + c_2 - c_0 \quad \text{and} \quad \lambda_1 = g \left(\frac{V_2 - V_0}{4} + \frac{c_2 + c_0}{2} \right)^2 \quad (4.24)$$

In zone 3 we have

$$v = \frac{2}{3} \left(\frac{y}{t} + \frac{V_2}{2} + c_2 \right) \quad \text{and} \quad \lambda = \frac{1}{9g} \left(V_2 + 2c_2 - \frac{y}{t} \right)^2 \quad (4.25)$$

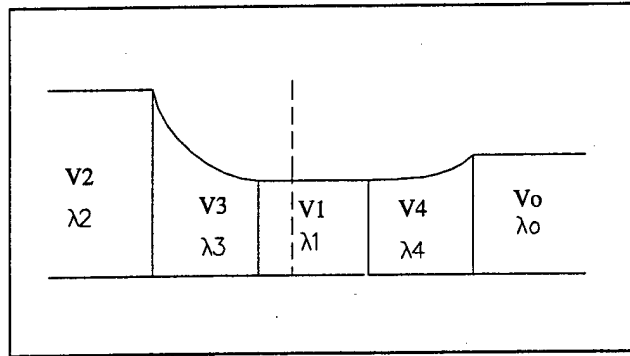


Figure 4-5: Solution for Riemann Problem Case III

where zone 3 is bounded by $(V_2 - c_2)t < y < (V_1 - c_1)t$. In Zone 4

$$v = \frac{2}{3} \left(\frac{y}{t} + \frac{V_0}{2} - c_0 \right) \quad \text{and} \quad \lambda = \frac{1}{9g} \left(2c_0 - V_0 + \frac{y}{t} \right)^2 \quad (4.26)$$

where zone 4 is bounded by $(V_1 + c_1)t < y < (V_0 + c_0)t$.

Solution to the Riemann Problem: Case IV

If $\lambda_0 = 0$ then the solution is a single rarefaction wave as in figure 4-6.

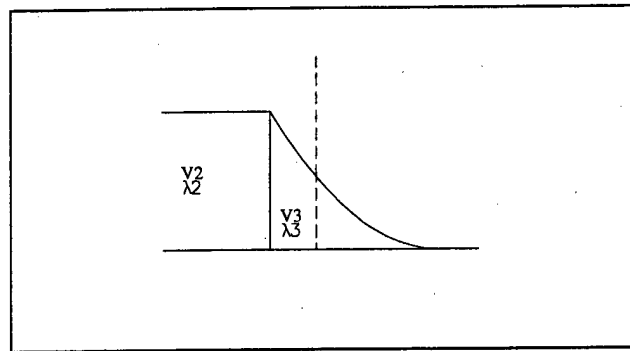


Figure 4-6: Solution for Riemann Problem Case IV

The solution in Zone 3 is

$$v = \frac{2}{3} \left(\frac{y}{t} + \frac{V_2}{2} + c_2 \right) \quad \text{and} \quad \lambda = \frac{1}{9g} \left(2c_2 + V_2 - \frac{y}{t} \right)^2 \quad (4.27)$$

where zone 3 is bounded by $(V_2 - c_2)t < y < (V_2 + 2c_2)t$.

Solution to the Riemann Problem: Case V

If in case III there is the additional condition that $V_2 + 2c_2 < V_0 - 2c_0$ then the water depth will be equal to zero in Zone 1 and the problem must be treated similarly to Case IV.

4.4 Selection of Water Motion on Deck Method

Computer programs for the flux difference splitting method and for Glimm's method were generated to solve a Riemann problem. The goal of this effort was to compare the methods to see which is most suitable for incorporation into the LAMP water on deck model. Figure 4-7 illustrates the solution to a Riemann problem using a first order flux difference splitting method scheme without flux limiters. The solid line is the exact solution, the other two lines are the numerical solutions. The line with the shorter dashes is for $\frac{\Delta t}{\Delta y} = \frac{0.005}{0.05}$ and the line with the longer dashes is for $\frac{\Delta t}{\Delta y} = \frac{0.001}{0.01}$. The scheme converges to the exact solution as Δy is made smaller.

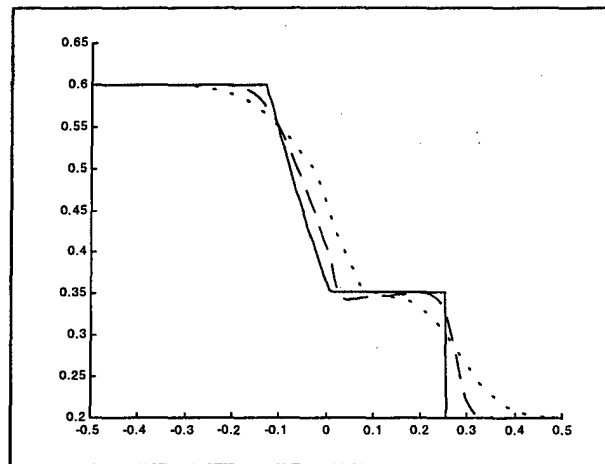


Figure 4-7: Riemann Problem Solution Using Flux Difference Splitting Method

Figure 4-8 illustrates the solution to the same Riemann problem using the Random choice method. The solid line is the exact solution, the other two lines are the numerical solutions.

The line with the shorter dashes is for $\frac{\Delta t}{\Delta y} = \frac{0.005}{0.05}$ and the line with the longer dashes is for $\frac{\Delta t}{\Delta y} = \frac{0.001}{0.01}$. This scheme also converges to the exact solution as Δy is decreased.

Due to the random interval sampling required in this procedure, the results vary each time the calculation is run. For example, for constant Δt , Δy , and initial conditions, a set of calculations will produce a unique solution curve for each calculation. Figure 4-9 shows three different solutions to a Riemann problem, the dashed lines, using the Random Choice Method. For each solution the initial conditions and calculation parameters were the same.

Other Riemann problems were investigated to compare the Random Choice and first order flux difference splitting methods. Table 4.1 summarizes a comparison of the two methods. An "X" entered in the Table means that method is superior to the other method in the given category.

Comparison Category	Random Choice Method	Flux Splitting Method
Ease of Programming		X
Accuracy for Given Discretization	X	
Repeatability of Solution		X
Ability to Capture Discontinuities	X	

Table 4.1: Comparison of Shallow Water Solution Methods

The flux difference splitting method was selected, primarily due to ease of programming, as the numerical method to be used for the for LAMP green water model.

4.5 Water Shipping Model

The difficulties in creating a realistic water shipping model are best framed by Dillingham in [6]. He states, 'In general the flow over the bulwark is very complicated since it results from the unsteady interaction between shallow water waves on the deck and deep water waves off the deck. In addition, direct observations of models indicate that the deck water may regularly impinge on the bulwark with considerable velocity and be thrown over the side in what amounts to a spray. To refer to this process as either turbulent or nonlinear is an understatement.'

For water shipping to occur, the height of the free surface at the ship side must exceed the height of the bulwark (or deck edge if there is no bulwark) and the relative velocity of the water above the top of the deck edge must be directed inward onto the deck. The height of the free

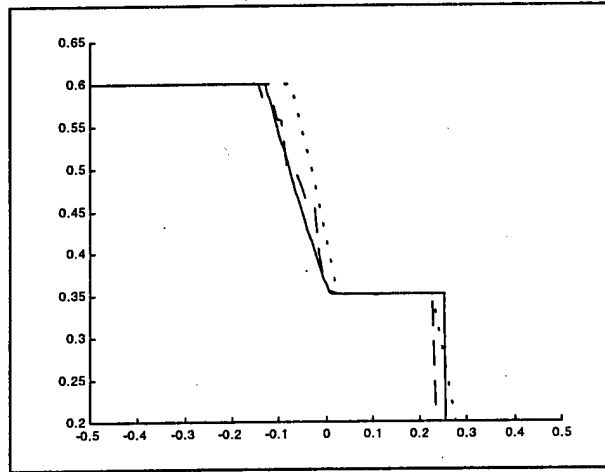


Figure 4-8: Riemann Problem Solution Using Random Choice Method

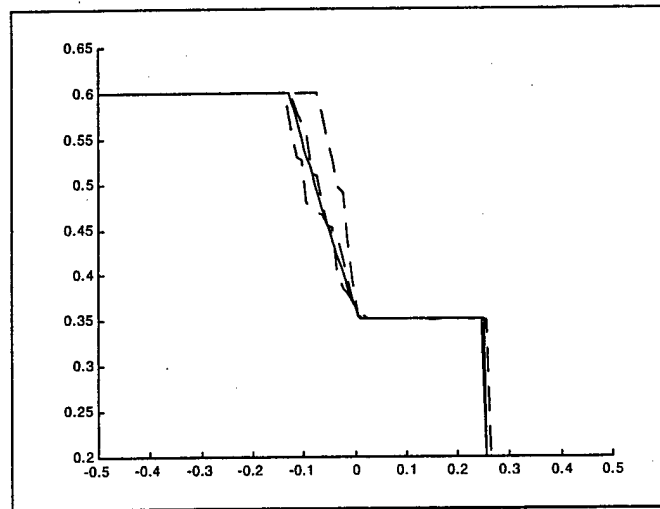


Figure 4-9: Solution Randomness in Random Choice Method

surface above the bulwark or deck edge is referred to as the relative elevation, η_R . This thesis makes use of a ship model with no bulwark so hereafter only the deck edge will be mentioned in the water shipping discussion. Figure 4-10 illustrates some geometries and variables used in the water shipping model. The XZ coordinate system represents the global system which maintains a fixed orientation. The primed system, X'/Z' , is the local coordinate system that moves with the ship. The variable η represents the free surface elevation and Z_d represents the height of the deck edge. Each is referred to the global system as a value along the z axis. The instantaneous relative elevation would be $\eta_R(t) = \eta(t) - Z_d(t)$. The vectors \vec{V}_{wx} and \vec{V}_{wy} are components of the water particle velocity \vec{V}_w . The vectors \vec{V}_{dx} and \vec{V}_{dy} are components of the deck edge velocity \vec{V}_d . All vectors are referred to the global system.

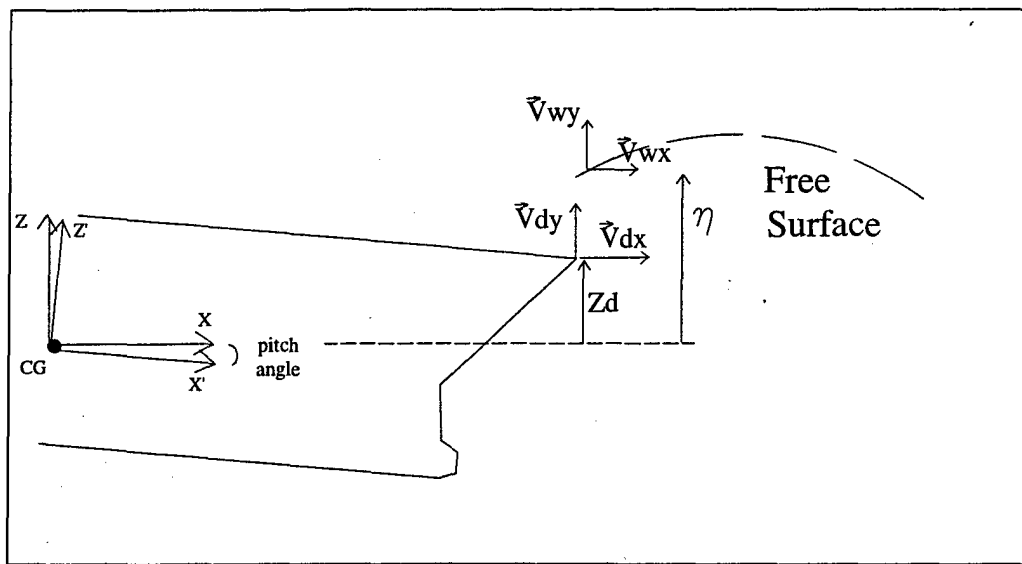


Figure 4-10: Geometry and Variables for the Water Shipping Model

4.5.1 Free Surface Elevation for Water Shipping

A basic description of the instantaneous free surface, $\eta(t)$, can be made by considering only the incident wave potential. However, for a more accurate description of the free surface around the ship hull the complete incident, diffracted, forward speed, and radiated wave system potentials should be used. The hydrodynamic potentials cause an increase in free surface elevation which

is commonly referred to as "pile-up" in the wave-body interaction. For a more complete estimation of pile-up the jet motion of the free surface from water-entry and slamming should be considered. In reference [8] a numerical technique for predicting the occurrence of water shipping is presented and it is concluded that the radiation and diffraction terms play important roles in the water shipping analysis and cannot be neglected.

For the water shipping model presented here, the incident wave potential is used for calculating the free surface height at the ship side. An elevation correction is then made to account for the forward speed, radiation, and diffraction potentials. The hull surface hydrodynamic pressure at the body panel adjacent to the waterline and nearest the desired deck location is used to compute an elevation which is added to the relative elevation computed from the ship motion and incident wave potential.

For a LAMP-2 calculation of the CG-47 hull in storm seas case, this elevation correction did not prove to be particularly large most of the time. It is probable that the correction would be larger for a LAMP-4 calculation, as the hydrodynamic calculation would include some hull flare effects.

4.5.2 Relative Velocity for Water Shipping

Several terms must be considered to determine the relative velocity, \vec{V}_r , of the water above the deck edge. The water particle velocity, \vec{V}_w , and ship velocity at the deck edge, \vec{V}_d , must be known. Also, an additional velocity due to the effect of hydraulic flow, V_h , must be included.

Hydraulic flow occurs due to energy conservation from converting the static head from the relative elevation into a velocity according to Bernoulli's equation. Referring to figure 4-11, where the variable z' is the local height off the weatherdeck, the static head height is $(\eta - Z_d) - z'$ and the hydraulic velocity is $V_h(z') = \sqrt{2g(\eta_R - z')}$. The hydraulic velocity is assumed to be directed onto the ship parallel with the x' axis. The dependency that V_h has on z' can be removed by averaging V_h over the static head. This is done with the following integral to obtain mass flow rate, Q ,

$$Q = \int_0^{\eta - Z_d} \sqrt{2g(\eta_R - z')} dz' \quad (4.28)$$

In [6] Dillingham uses a technique similar to equation 4.28 to integrate for the mass flow rate onto a ship's weatherdeck. Carrying out the integration in 4.28 and then dividing by the static

head height to obtain an average hydraulic flow, $V_{h_{ave}}$, gives

$$V_{h_{ave}} = \frac{2}{3} \sqrt{2g\eta_R} \quad (4.29)$$

The water shipping model, then, uses $V_{h_{ave}}$, \vec{V}_w , and \vec{V}_d for the relative velocity calculation.

The calculation for $V_{h_{ave}}$ is a simplification made for this thesis. In reference [11] the hydraulic flow contribution to water shipping is treated within a more general calculation for mass of the wave shipped on deck. The mass calculation is performed by integrating around the edge, L , of the weatherdeck as follows,

$$Mass = \rho \int_0^t \oint_{JL} C_o \left[\int_0^{\eta_R} (\vec{V}_w - \vec{V}_d) dz + \int_0^{\eta_R} V_h(z) dz \right] dl dt \quad (4.30)$$

The constant C_o in equation 4.30 was determined experimentally by Grochowalski to be 0.55.

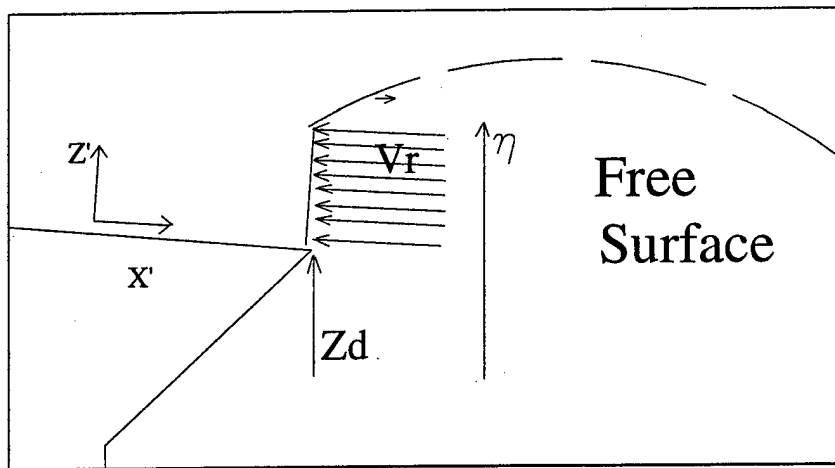


Figure 4-11: Water Shipping

Because \vec{V}_w and \vec{V}_d are vector quantities, the calculation for \vec{V}_r can be performed several different ways depending on the assumptions made. These calculations will be referred to as Methods I, II, and III. In any case, since shallow water theory assumes all fluid velocity is parallel with the deck surface, the direction for \vec{V}_r , shown in figure 4-11, is always considered to be parallel with the weatherdeck. For Method I, the calculation will use only the horizontal

components of the wave and particle velocities so that

$$V_r = V_{d_x} - V_{w_x} + V_{h_{ave}} \quad (4.31)$$

For Method II, the calculation will consider the ship's instantaneous pitch angle, Θ , and use the components of the vectors \vec{V}_{w_x} , \vec{V}_{w_y} , \vec{V}_{d_x} , and \vec{V}_{d_y} that are parallel with the $x/$ axis. The calculation for V_r in this case is

$$V_r = V_{d_x} \cos(\Theta) - V_{d_y} \sin(\Theta) - (V_{w_x} \cos(\Theta) - V_{w_y} \sin(\Theta)) + V_{h_{ave}} \quad (4.32)$$

The Method III calculation will be performed by conserving the momentum of the water particle. For long crested head seas there are only two wave particle velocity components so that

$$V_r = V_{d_x} \cos(\Theta) - V_{d_y} \sin(\Theta) \pm \sqrt{V_{w_x}^2 + V_{w_y}^2} + V_{h_{ave}} \quad (4.33)$$

where the plus (+) is used when $(V_{w_x} \cos(\Theta) - V_{w_y} \sin(\Theta)) < 0$ and the minus (-) is used when $(V_{w_x} \cos(\Theta) - V_{w_y} \sin(\Theta)) > 0$.

The relative velocity and elevation must be calculated at each time step. As indicated in figure 4-11, the velocity is considered to be a constant from the deck edge to the top of the free surface. With the relative velocity and elevation of the water at the deck edge known, they can be considered as boundary conditions for a water on deck problem. When the relative elevation becomes negative, the boundary conditions are set to zero. Evolving the water-on-deck problem through time, with the relative velocity and elevation boundary conditions updated at each time step, will result in mass flow onto the deck. Water shipping, therefore, is treated as a boundary condition to the water on deck problem.

4.6 Green Water Model in LAMP

To create a green water model in LAMP for head seas, a weatherdeck was included in the hull geometry description. The deck was modeled as a surface projecting aft from the ship bow a distance approximately 25% of the overall ship length. The weather deck is divided into strips of width *dely*. At the center of each strip is a deck edge reference point at which data

needed for the water shipping problem is calculated. Figure 4-12 illustrates this setup. The

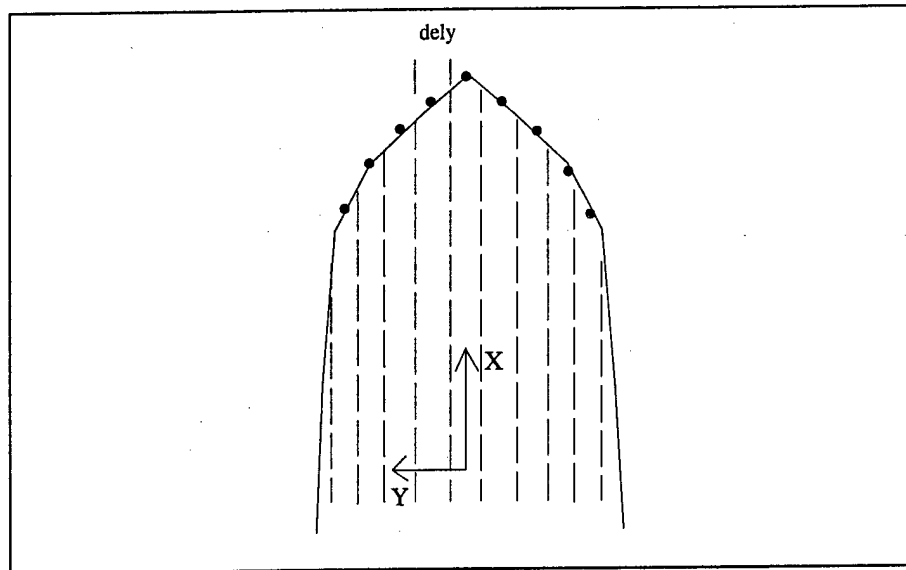


Figure 4-12: Weatherdeck Division for LAMP Green Water Model

model uses the flux difference splitting method to solve the shallow water problem in each strip as a two-dimensional free surface. Transverse water flow (from one strip to another) is not calculated.

A LAMP subroutine was provided by SAIC to calculate, at each time step, the deck edge motion, deck edge location, free surface height, and incident wave particle velocity for each reference point shown in figure 4-12. With this data, the relative elevation and velocity can be determined for each deck edge point.

After solution of the shallow water problem for each strip at each time interval, the forces, moments, and the time-dependent mass and mass moment of inertia terms in the dynamic equations of motion can be calculated that result from the water on deck. Because of the time-dependent mass terms in the dynamics equations of motion, the green water on deck is treated as part of the rigid body. Thus the only green water induced forces and moments that need to be calculated for rigid body motion are those due to gravity acceleration. For the local loads on the weatherdeck and superstructure, however, the absolute green water fluid acceleration in the local coordinate system must be calculated. Let \vec{a}_{GW} be the absolute acceleration of the

green water in the local ship coordinate system. As defined previously \vec{V} is the rigid body velocity at cg and $\vec{\omega}$ the rigid body rotation. Then from simple dynamics

$$\vec{a}_{GW} = \frac{d\vec{V}}{dt} + \frac{d\vec{\omega}}{dt} \times \vec{r}' + \vec{\omega} \times (\vec{\omega} \times \vec{r}') + 2\vec{\omega} \times \vec{v}' + \vec{a}_{rel} \quad (4.34)$$

where \vec{r}' and \vec{v}' is the position and velocity, respectively, of the green water referred to the local coordinate system. The vector \vec{a}_{rel} is the acceleration of a point in the green water measured relative to the local frame by an observer attached to the local frame. This quantity is zero for the green water problem. The vertical acceleration component of \vec{a}_{GW} is defined as a_z' . At each time step a_z' can be calculated for the green water on deck as a function of the x axis in figure 4-12. The total deck pressure, P_{deck} , is then be calculated by including the gravity static head, which must include pitch angle, and the depth of the green water, ζ , so that

$$P_{deck} = \rho\zeta (a_z' + g \cos(\Theta)) \quad (4.35)$$

Forces from green water on large superstructure, where the water particle velocity at the structure boundary can be approximated as zero over a wide area, can be calculated from equation 4.35 by integrating the pressure through the water column. For smaller weatherdeck structures a better estimate of the local green water loads may be made by considering the green water particle velocity.

Figure 4-13 visualizes a solution to the green water problem by plotting the water depth for one strip over a series of time steps with a sinusoidal incident wave. In this case the ship is moving to the right into the sea, the bow is on the right, and time is increasing with the higher curves. The horizontal portion of each curve is an area where the deck is dry.

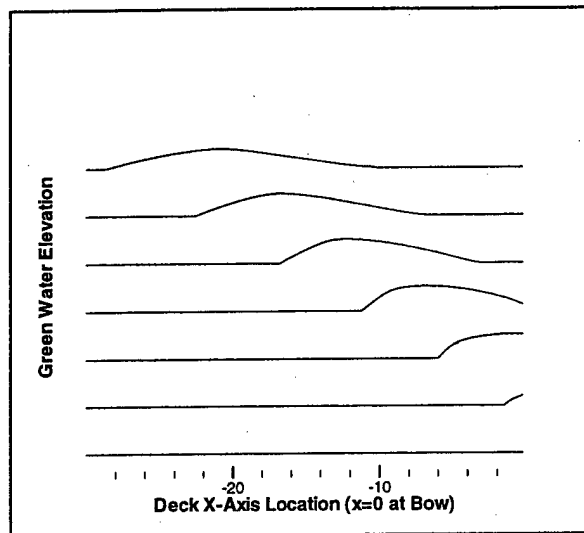


Figure 4-13: Flow Visualization of Green Water on Deck

Chapter 5

Validation and Results

5.1 Validation

5.1.1 Validation of Dynamic Equation of Motion Solver

The changes to the LAMP dynamic equations of motion to include time-dependent mass and moment of inertia were validated using the model shown in Figure 5-1. The model is a body with two lumped masses, M_o , at the ends of a massless rod. The body has initial linear velocity

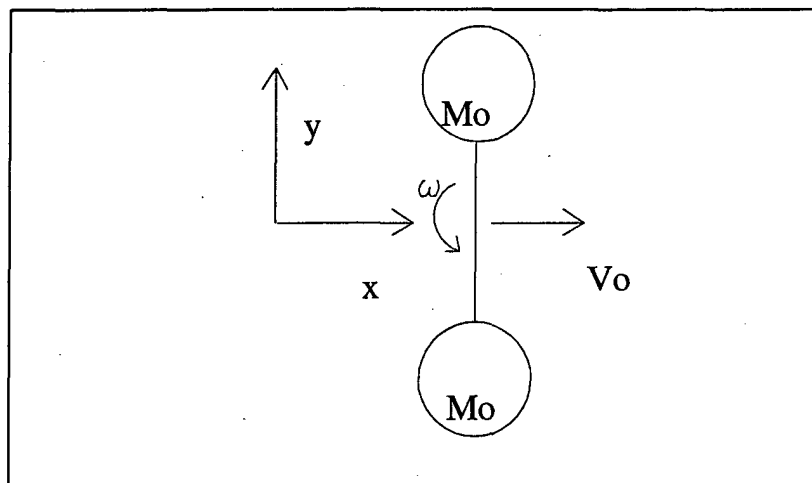


Figure 5-1: Model Used to Validate Dynamic Equations of Motion Solver

V_o and initial angular velocity ω whose vector representation is pointed along the x axis. The

solution for linear and angular velocity over time was calculated as the mass was reduced at a constant rate. At time $t = 0.5$ the mass reduction was ceased. The results in figures 5-2 and 5-3 show linear momentum, \vec{P} , and angular momentum, \vec{H} , is conserved in the calculation. In each figure, the horizontal line is the constant momentum and the slanted line is either the mass (figure 5-2) or the moment of inertia (figure 5-3). The parabolic line is either the linear velocity (figure 5-2) or the angular velocity (figure 5-3).

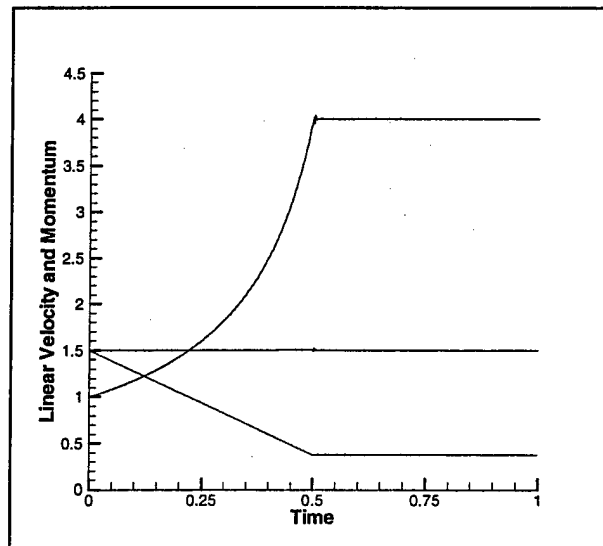


Figure 5-2: Conservation of Linear Momentum

5.1.2 Validation of Compartment Flooded Volume and Moment of Inertia Calculation

The flooded compartment module added to LAMP calculates volume, mass center, and moment of inertia. The module also calculates a final hydrostatic position after flooding is complete in any number of specified compartments. These calculations were validated by running them with a rectangular hull geometry input. Separate calculations were made with the same rectangular hull using different calculation methods and software. Results from the LAMP module agreed with results from the independent method to within 99%.

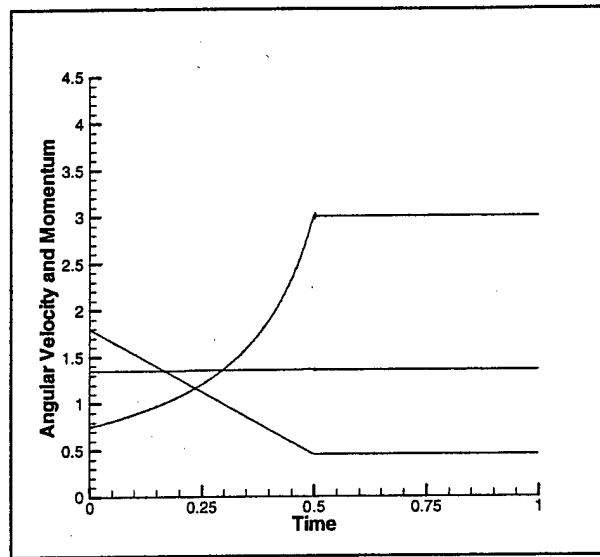


Figure 5-3: Conservation of Angular Momentum

5.1.3 Validation of Flux Difference Splitting Method

A bore propagation problem is solved to validate the flux difference splitting method used for the water motion on deck problem. In particular, this problem validates the homogeneous form of the difference scheme, equation 4.6. The initial conditions are a Riemann Problem

$$\left. \begin{array}{l} v = 0.2667 \\ \lambda = 10.8 \end{array} \right\} y < 0 \quad \text{and} \quad \left. \begin{array}{l} v = 1.6 \\ \lambda = 1.8 \end{array} \right\} y > 0 \quad (5.1)$$

where the velocity units are m/s and the water height units are m . The exact solution to the problem for water depth has been given by Stoker in [30]:

$$\lambda(y, t) = \begin{cases} 10.8 & \text{for } y < -10.0t \\ \frac{1}{88.2} \left(20.84 - \frac{y}{t} \right)^2 & \text{for } -10.0t < y < 0.45t \\ 4.716 & \text{for } 0.45t < y < 10.7t \\ 1.8 & \text{for } y > 10.7t \end{cases}$$

The exact solution shows that a bore travels in the positive y -direction with a velocity of $10.7 m/s$, and a rarefaction wave propagates in the negative y -direction at a speed of $10.0 m/s$.

Figure 5-4 shows the numerical results (dashed line) and the exact solution (solid line) for the water depth. The numerical results match well with the exact solution. Because the numerical scheme is first-order, it has some difficulty handling the shock front. This is evident in lost resolution and that the shock front travels slightly faster than the exact speed. This can be corrected with a higher order scheme.

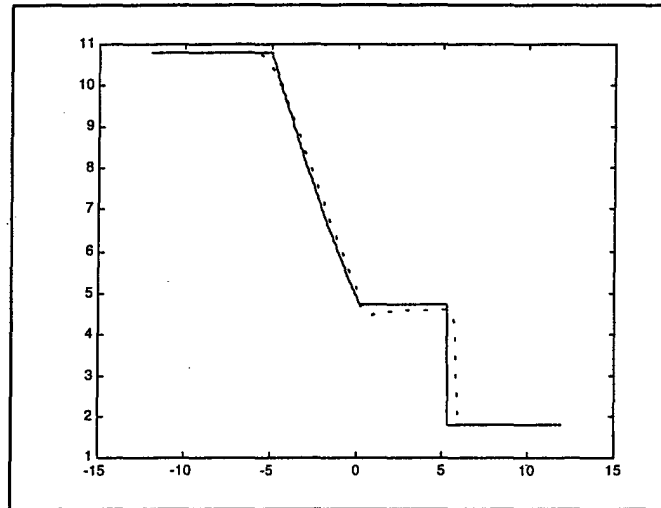


Figure 5-4: Bore Propagation at $t = 0.5$ seconds

A second problem was used to validate the flux difference splitting method when the ship is undergoing motion. Mathematically this is the condition where the right hand side of equation 4.1 is non-zero. This problem, then, is a test on the numerical scheme used for equation 4.12. The problem is one solved by Huang and Hsiung in [12] for sloshing inside a deck well. The computations are carried out for the deck flow excited by roll motion. The deck is 1 meter wide, oscillating about a pivot which is 0.522 meters above the deck, and the roll amplitude is 0.067 rad. The mean water depth is 6 cm. The primary resonant frequency of the shallow-water motion inside the deck well is $\omega_o = 2.41 \text{ rad/sec}$. The numerical results in figure 5-5 are for a rolling frequency of $\omega = 0.9 \text{ rad/sec}$, well below resonance, to show the water behaves as a "horizontal surface." The rolling frequency was then increased to twice the resonance frequency and results plotted in figure 5-6. At this frequency, standing waves are formed with the wave length approximately equal to the deck width. In each figure, plots were made of the

free surface at several time instances to illustrate the motion.

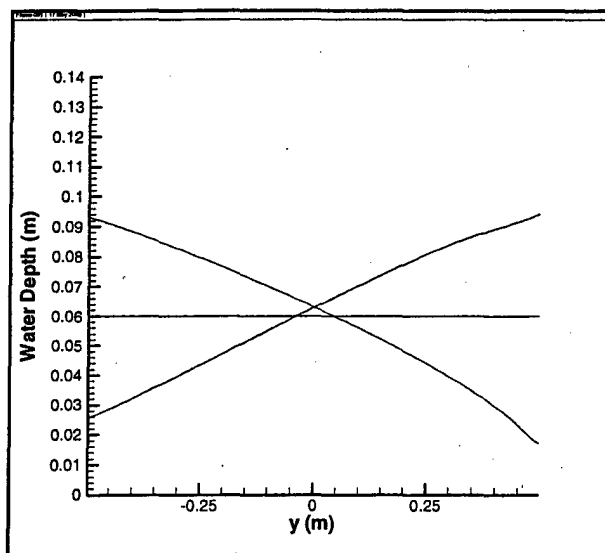


Figure 5-5: Shallow Water Sloshing Below Resonant Frequency

5.2 Results for Flooding Models

This section provides some results from the compartment flooding model that was added to LAMP. In all cases, unless noted otherwise, the LAMP-2 formulation was used. The results include effects on roll and pitch motions from a flooded volume and examples of inaccuracies that arise due to a shifting cg and due to a changing mean body boundary position when linear hydrodynamics are used. The ship model that was run in LAMP for these results is a CG47 Class Cruiser. A steady forward speed of 10 knots was used for all the calculations. This ship model was used on the recommendation of SAIC due to its excellent past performance.

All plots of ship motion were made in non-dimensional units. If the ship has length L then linear motions are made non-dimensional by dividing by L and time is made non-dimensional by dividing by $\sqrt{\frac{L}{g}}$. Angular motions are plotted in radians.

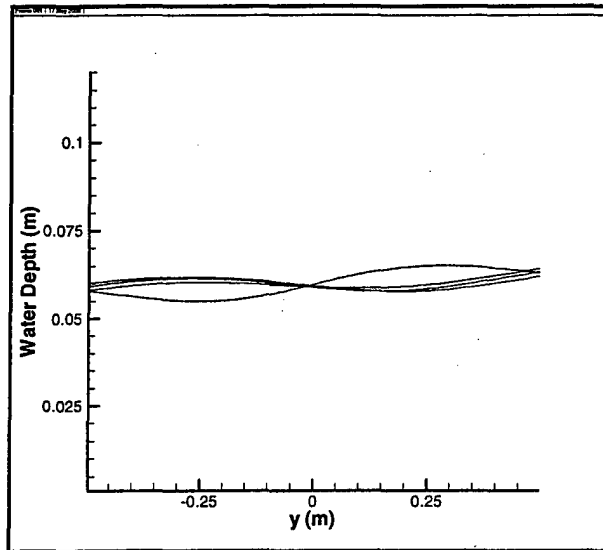


Figure 5-6: Shallow Water Sloshing, Twice Resonance Frequency

5.2.1 Roll Motion Results

The first results, figures 5-7 and 5-8, show the effect of flooding and sloshing on roll motion. Beam seas with a single sinusoid wave component were used to induce ship roll motions. A large amidships compartment with length equal to 20% of ship length was created for flooding. The bulkhead locations were at 0.4 and 0.6. Figure 5-7 illustrates roll motion of the intact hull (solid line) and of the flooded ship (dashed line). For the flooded ship, the problem was started with the ship in its final flooded position from uncontrolled flooding into the compartment and sloshing was not included in the calculation. The linear hydrodynamics and sinusoid seaway cause the motion to reach steady state after the starting transients pass. The roll motions of the flooded ship are much reduced compared to the intact ship due to the flooded mass having lowered the ship's *cg*. Sloshing effects were then added to the calculation. Figure 5-8 compares roll motion of the flooded ship without sloshing (solid line) and with sloshing (dashed line). The sloshing causes a roll moment, the effects of which can clearly be seen in the increased roll amplitude.

5.2.2 Vertical Motion Results

The next set of results, figures 5-9 and 5-10, show the effect of flooding on vertical motion and relative elevation at the bow. Head seas with a single sinusoid wave component were used to induce pitch and heave motions. The wavelength was set at 1.5 times the ship length to excite pitch motion. Wave amplitude was 17 feet to approximate about a sea state 6. These extremely harsh conditions were intentional to create a large relative elevation at the bow for water shipping. A forward compartment with bulkhead locations 0.1 and 0.25 was created for flooding. Figure 5-9 illustrates pitch motion of the intact hull (solid line) and of the flooded ship (dashed line). For the flooded ship, the problem was started with the ship in its final flooded position from uncontrolled flooding into the compartment. The trim of the flooded ship is indicated in the initial pitch angle. Sloshing was not included in any of the pitch calculations. The effects from the longitudinal moment induced by the flooded water and its moment of inertia can be seen in the flooded ship motions. Notice that the flooded ship spends a greater amount of time than the intact ship with the bow pitched downwards (positive pitch angle). In such a condition shipping water is more likely to occur which is why a green water model is also necessary for LAMP to be used as a damage stability prediction tool. There is little difference in the intact and flooded ship heave motions for the same flooding scenario. Figure 5-10 illustrates this motion for the intact ship (solid line) and flooded ship (dashed line). The motions are similar but the flooded ship's vertical position is offset due to its lower cg.

The relative height of the bow deck edge above the instantaneous free surface¹ is calculated for water shipping and can be plotted for the pitch motions in figure 5-9. This relative bow height is shown in figure 5-11 for the intact ship (solid line) and the flooded ship (dashed line). Shipping water occurs during a negative relative bow height (positive relative elevation). The time duration and magnitude of each shipping water event is greater for the flooded ship.

5.2.3 Loss of Accuracy Examples

Possible causes for loss of accuracy in the LAMP flooding simulation calculation have been discussed and examples are now provided. The next set of results shows that a changing mean

¹The term "relative elevation" was used in the green water model discussion as meaning the free surface height minus the deck height, the relative bow height is just the negative value of the relative elevation.

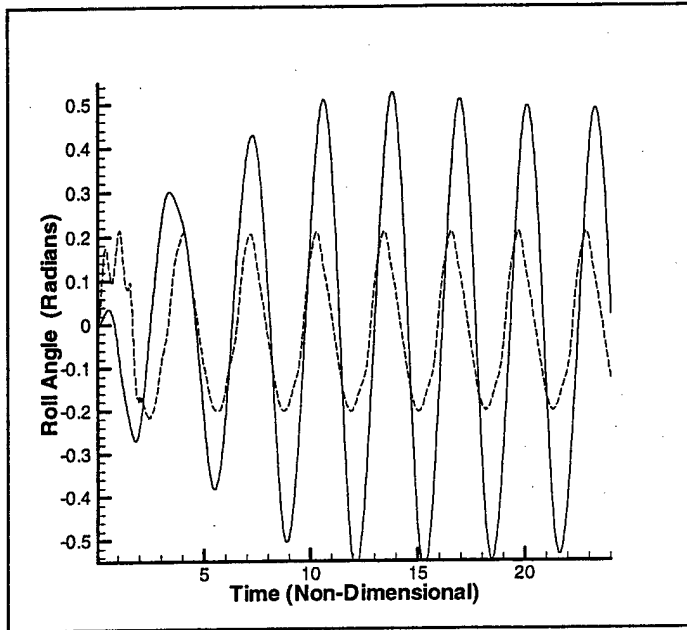


Figure 5-7: Roll Motion Intact and Flooded Ships

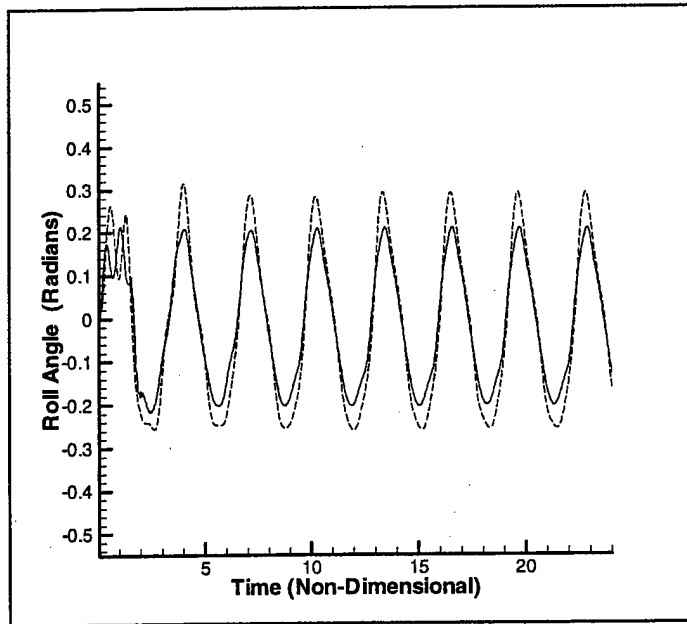


Figure 5-8: Sloshing Effects on Roll Motion

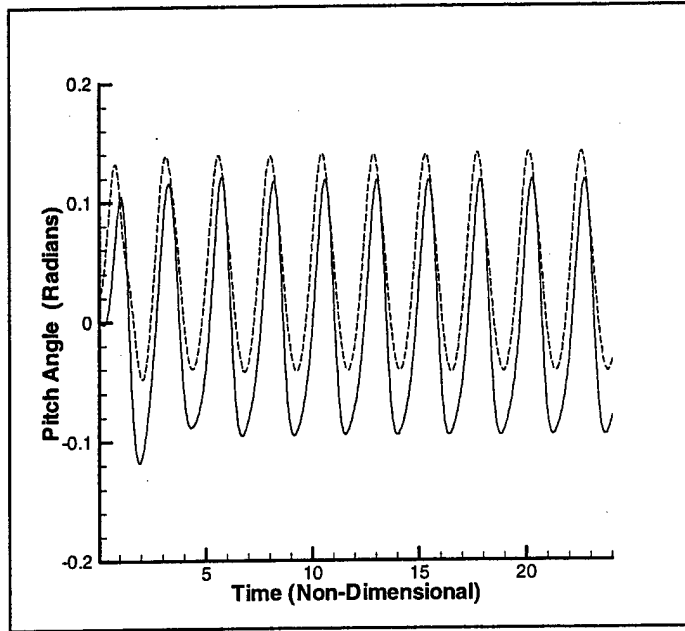


Figure 5-9: Pitch Motion Intact and Flooded Ships

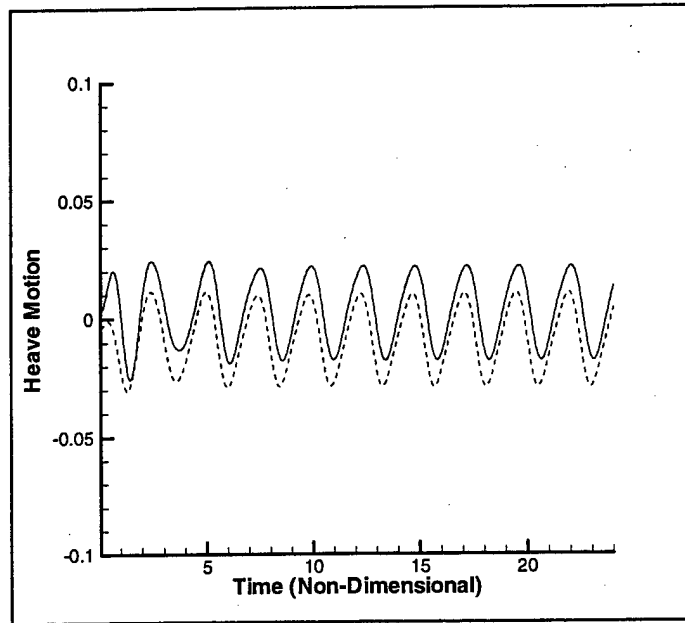


Figure 5-10: Heave Motion Intact and Flooded Ship

body boundary position affects linear calculation accuracy and also that a shifting **cg** introduces errors in the angular motion calculation. Figure 5-12 plots pitch motion to illustrate loss of linear calculation accuracy. For each curve in the figure the problem was started with the ship in its final flooded position from uncontrolled flooding in the forward compartment bounded by the 0.1 and 0.25 bulkheads. The seaway conditions were the same as the conditions for the figure 5-9 simulation. The solid curve is the accurate linear hydrodynamic calculation; it used the final flooded hydrostatic position as the mean body boundary position. The dashed curve used the ship's intact (non-flooded) mean body position for the linear hydrodynamic calculation. This example shows the calculation with the incorrect mean body position overestimates the peak positive pitch by approximately 0.5 degrees.

Figure 5-13 illustrates the effect on angular motion calculation due to a shift in **cg**. For each plot the problem was started with the ship in its final flooded position from uncontrolled flooding in the forward compartment bounded by the 0.1 and 0.25 bulkheads. This flooded condition moves **cg** forward by 3.8% and down 0.23% of ship length from its initial intact position. The seaway conditions were the same as the conditions for the figure 5-9 simulation. The solid curve is the pitch motion where the ship's **cg** was moved prior to the start of the calculation to account for the flooded water. The dashed curve is the same calculation except that the ship's **cg** was only moved longitudinally to account for the flooded water. It was not moved vertically.

5.2.4 Progressive Flooding Results

The last flooding simulation result is an example of progressive flooding. The seaway conditions were the same as the conditions for the figure 5-9 except that the wave amplitude was reduced by two thirds. The problem was started with the ship in its final flooded position from uncontrolled flooding in the forward compartment bounded by the 0.1 and 0.25 bulkheads. At time equal to 12, indicated by "start" in figure 5-14, flooding at a constant rate was initiated into a compartment bounded by bulkheads 0.25 and 0.4. At time equal to 24, indicated by "stop" in figure 5-14, flooding ceased. Figure 5-14 plots the pitch and heave motions, the heave motion is the lower curve in the figure. Figure 5-15 plots the relative bow height during the progressive flooding simulation. Note that shipping water events do not occur until the

progressive flooding commences.

As a comparison, this progressive flooding simulation was run a second time using the fully non-linear LAMP-4 formulation. The linear and non-linear calculation results for pitch motion and relative bow height are plotted in figures 5-16 and 5-17. The non-linear calculation results are plotted as solid lines, the linear as dashed lines. The results for the two calculation methods have close agreement. As before, however, the calculation with the less accurate mean body boundary position (linear calculation) overestimates the pitch motion.

5.3 Results for Green Water

This section provides some results from the green water model that was added to LAMP. In all cases the LAMP-2 formulation was used. The results include effects on vertical motions from green water and plots of green water mass and local deck loads. A CG47 Class Cruiser at a steady forward speed of 10 knots was used for the calculations. Plots of ship motion, mass, and mass centers are made in non-dimensional units. Because the CG47 is such a massive ship, the density of the green water used in calculations for all of the results below was increased by a factor of five. This was done to make the green water mass and its effects on ship motion stand out.

Head seas with a single sinusoid wave component were used. The wavelength was set at 1.5 times the ship length to excite pitch motion. Wave amplitude was 14 feet. This amplitude was determined through trial and error to provide about a 10 foot relative elevation for the water shipping problem. Relative elevations higher than this required increased calculation time because smaller time steps were needed to solve the shallow water problem. Also, for relative elevations much larger than 10 feet it was found that large time-dependent mass and moment of inertia terms were calculated that caused the dynamic equations of motion solution to break down.

Figure 5-18 shows the effect of green water on pitch motion. This figure plots the relative bow height and pitch motion of a LAMP calculation with no green water effects (solid lines) and with green water effects (dashed lines). The relative bow height is the curve with smaller negative amplitudes. The increased angular inertia of the ship with the green water delays its

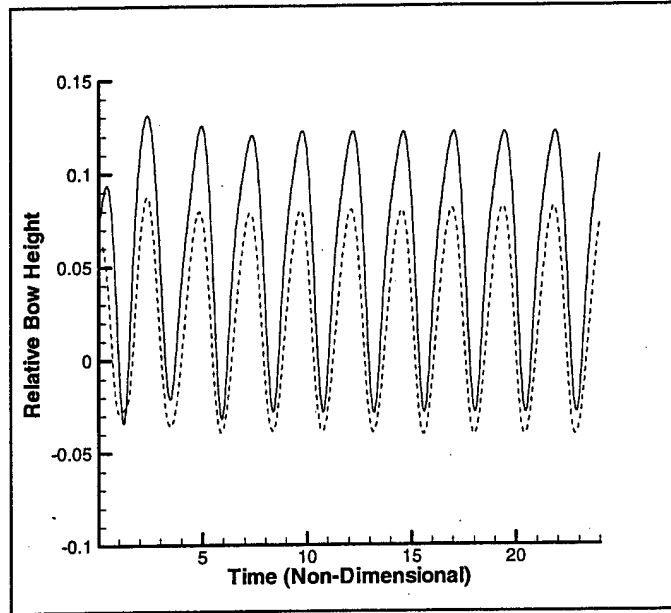


Figure 5-11: Flooding Forward, Bow Height Above Free Surface

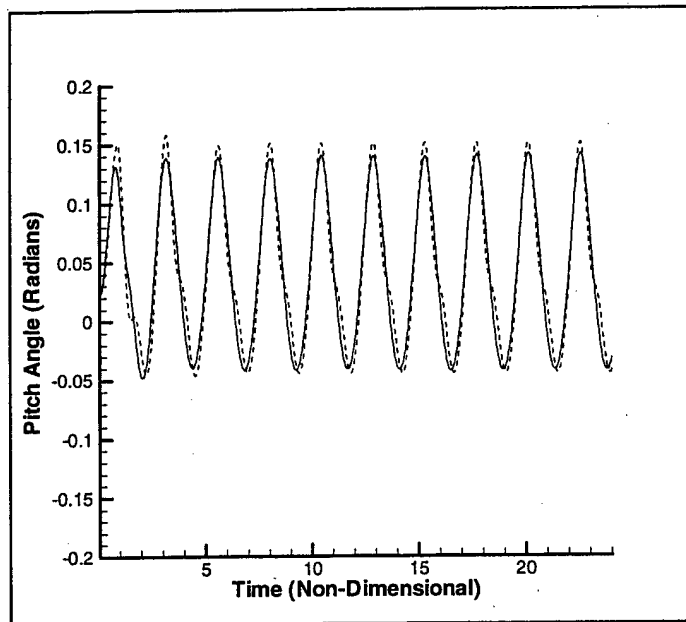


Figure 5-12: Effects of Linear Hydrodynamics and Flooding

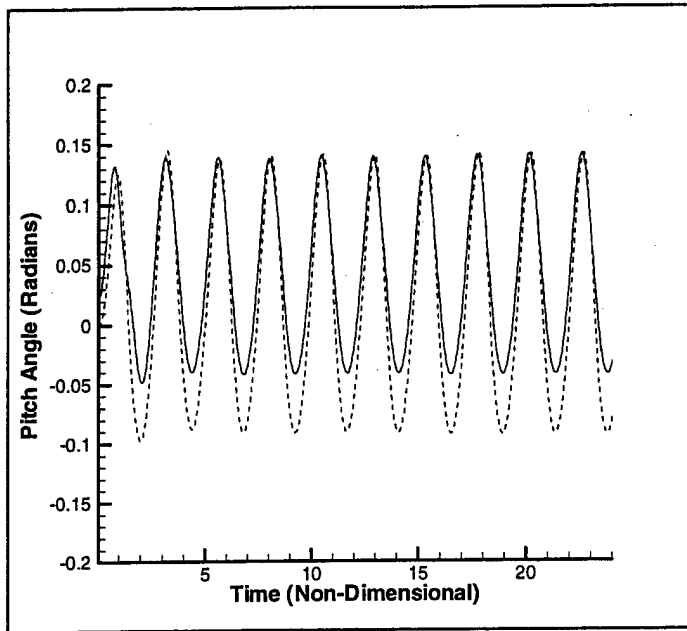


Figure 5-13: Effect of Center of Gravity Shift on Pitch Motion

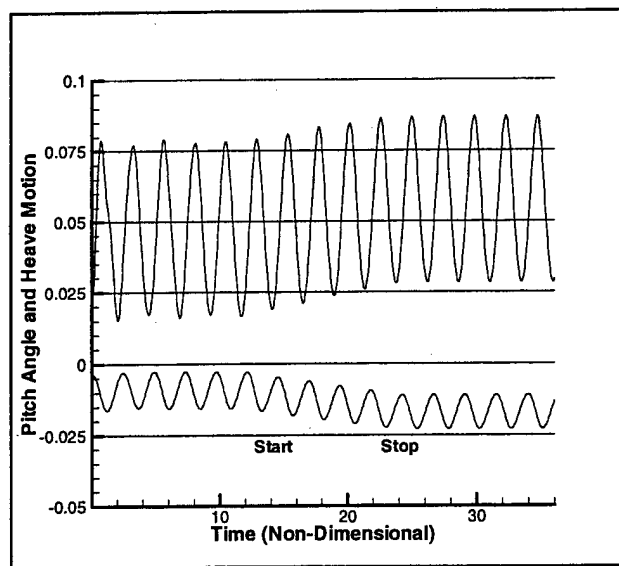


Figure 5-14: Progressive Flooding Pitch and Heave Motion

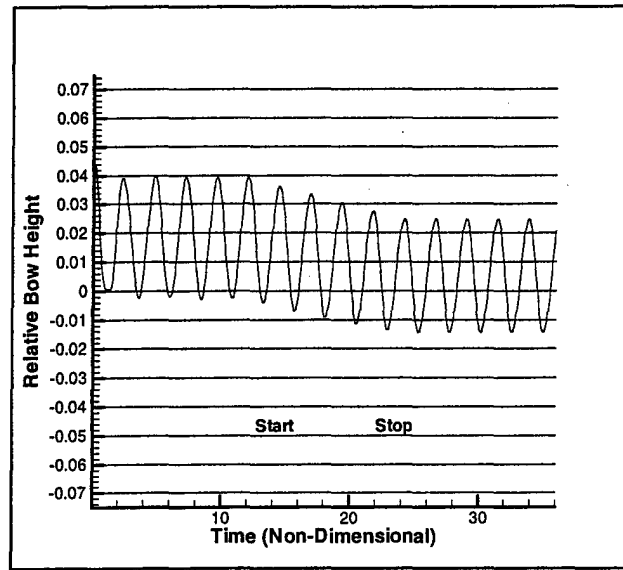


Figure 5-15: Progressive Flooding Relative Bow Height

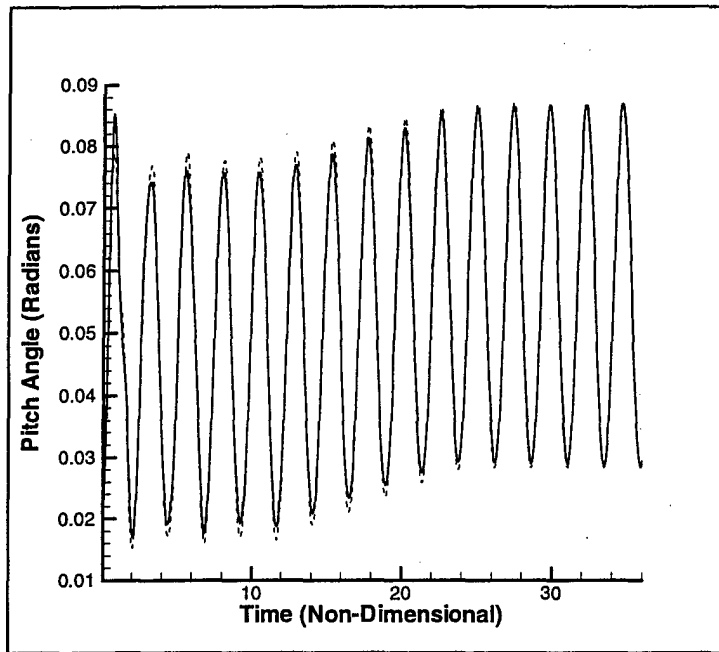


Figure 5-16: Linear and Nonlinear Progressive Flooding Pitch Motion Calculation

motion response to the incoming waves and slightly increases the maximum amplitude of the positive pitch motion. Figure 5-19 shows the effect of green water on heave motion. Heave motion is slightly increased in the motion calculation that includes green water (dashed line). Again, the green water density was artificially increased by a factor of five for these results. For smaller ships and craft the green water would have a much larger effect on pitch motion. Green water simulations were not run for beam seas but roll amplitudes would probably also be enhanced due to a greater tendency of a ship to roll than pitch.

The calculation for \vec{V}_r in the water shipping problem was performed using Methods I, II, and III. Figure 5-20 plots relative bow height (the sinusoidal curve) and green water mass on deck for two water shipping events using Method I for water shipping problem. The green water mass was normalized by dividing it by the ship mass. A second calculation using Method II for the water shipping problem showed no discernible differences from the Method I calculation results. The amount of green water mass shipped on board in each calculation was the same.

The Method III calculation for shipping was based on conserving momentum of the incoming wave. Figure 5-21 plots the green water mass on deck using Method III (dashed line) and the green water mass using Method I (solid line). The Method III calculation for shipping water velocity should be the method normally used because it results in the most green water mass on deck; it provides the most conservative estimate of water shipping.

The green water model solved the water-motion-on-deck problem in strips of width *dely* assuming a two-dimensional free surface. This approach prevents transverse water flow so that no green water is able to fall off the port and starboard sides of the weatherdeck. Therefore the time-duration that the green water mass is calculated to be on the weatherdeck is longer than the time-duration if a three-dimensional free surface were solved. For three-dimensional calculations, the green water mass curve would have about the same peak value but would go to zero after each water shipping event in a shorter amount of time. It would have more of a spiked appearance.

The green water mass center location and local deck loads are also presented. Figure 5-22 plots mass and mass center for two water shipping events. The weatherdeck longitudinal coordinate between 0.4 and 0.5 corresponds to the bow area. The aft end of the weatherdeck has coordinate 0.25. Figure 5-23 plots local deck pressure due to green water and pitch angle

(sinusoidal plot). The dashed line is pressure for a location at the bow, the solid line is pressure for a location aft of the bow a distance 0.06 (non-dimensional). The green water pressures are normalized by dividing them by the hydrostatic head of the green water, $\rho g \zeta$, where ζ is the green water depth. This figure shows that the green water deck pressure increases by almost a factor of two over hydrostatic during peak accelerations in pitch motion.

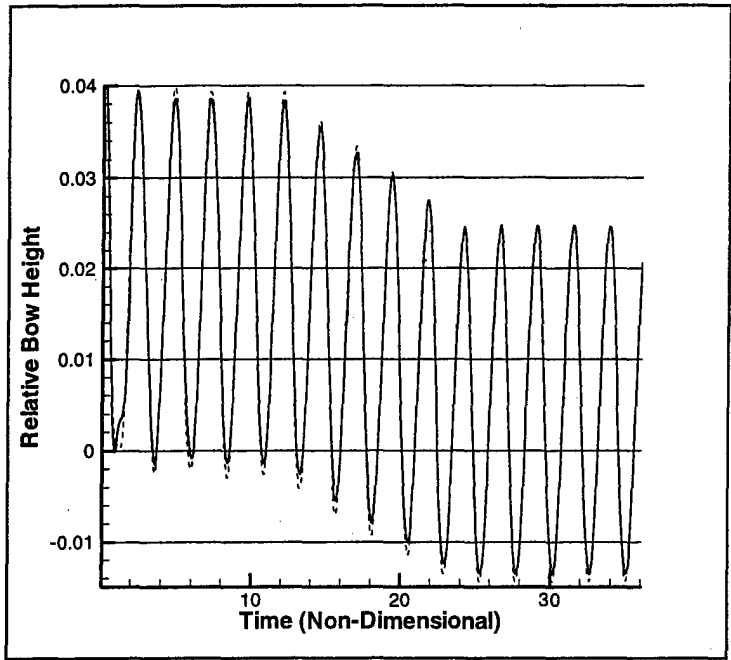


Figure 5-17: Linear and Nonlinear Progressive Flooding Relative Bow Height Calculation

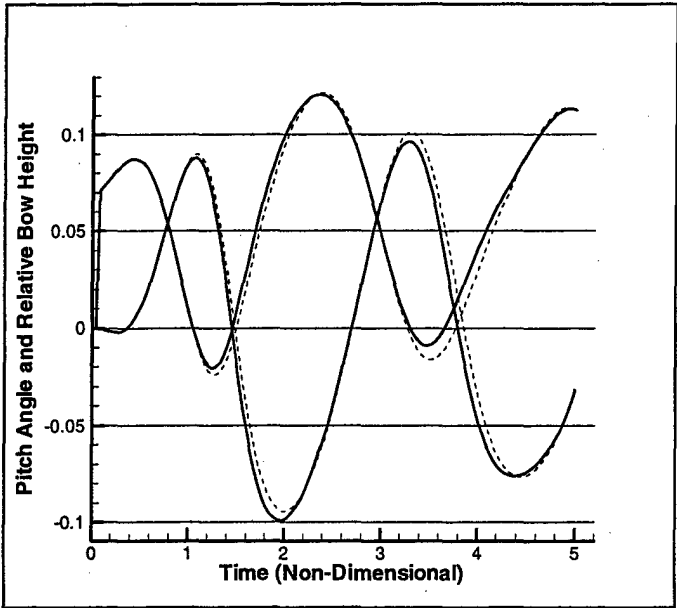


Figure 5-18: Effects of Green Water on Pitch Motion

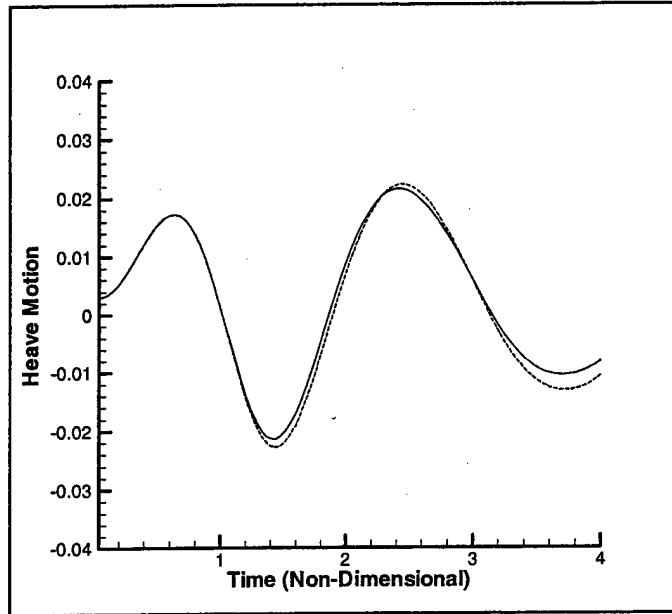


Figure 5-19: Effects of Green Water on Heave Motion

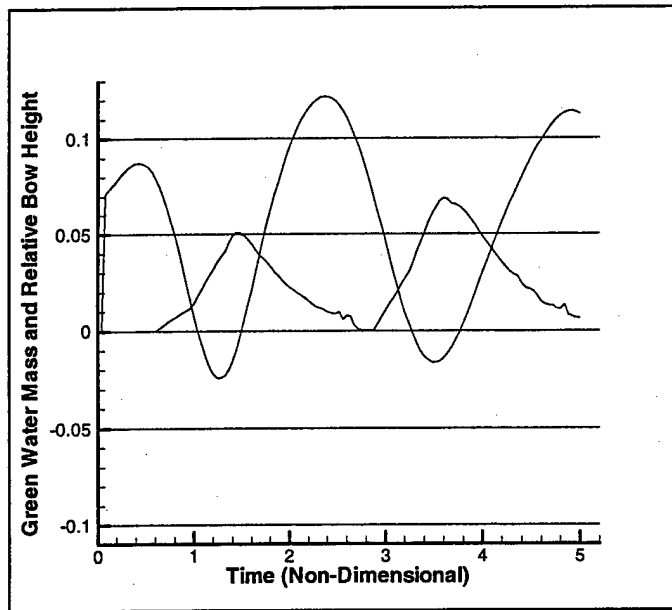


Figure 5-20: Relative Bow Height and Green Water Mass on Deck

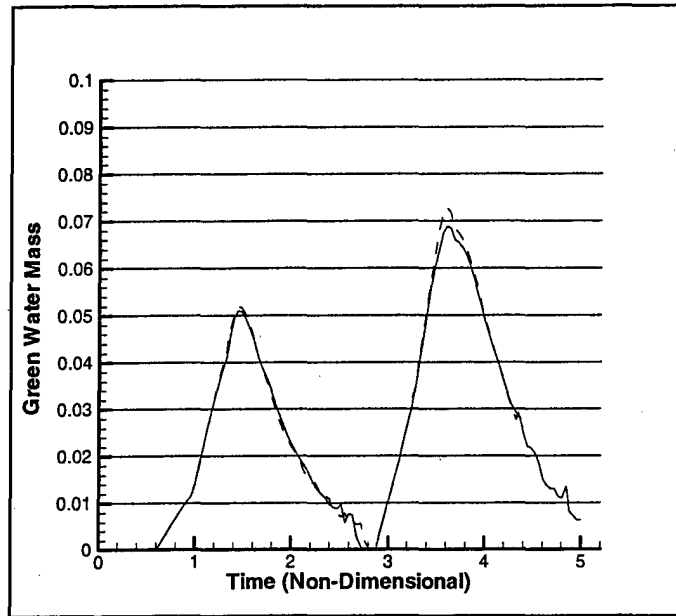


Figure 5-21: Mass on Deck Using Different Shipping Water Velocities

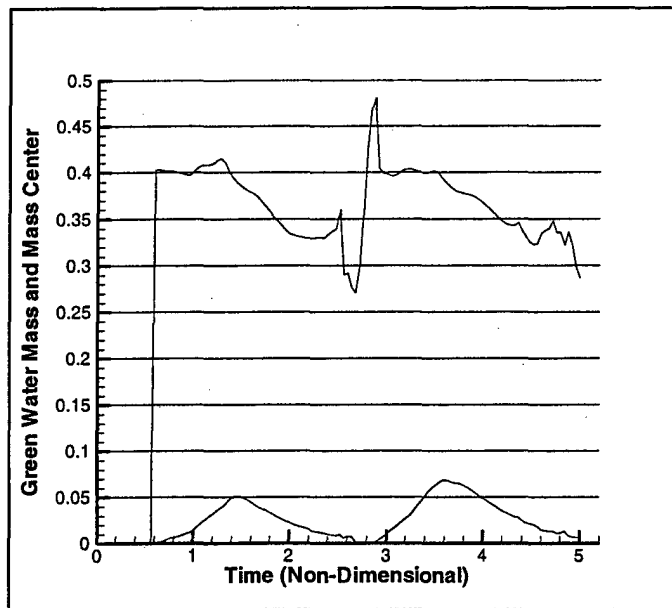


Figure 5-22: Green Water Mass on Deck and Mass Center

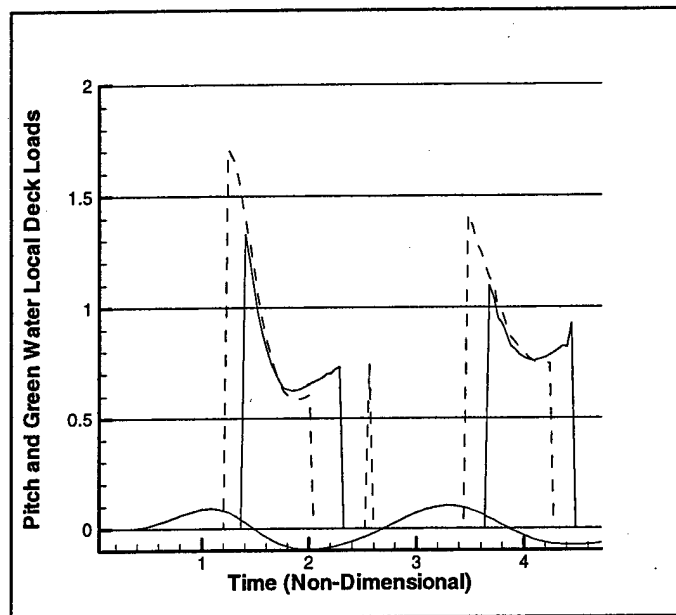


Figure 5-23: Pitch Motion and Local Green Water Deck Loads

Chapter 6

Conclusions

6.1 Discussion and Recommendations

This research investigated the addition of models for compartment flooding and green water to the LAMP time-domain ship motion program so that it could be used as a damaged stability prediction tool. The approach was to treat both events, the flooded water and the green water on the weatherdeck, as a change in the ship rigid body mass. Time-dependent mass and mass moment of inertia terms were calculated for the water and incorporated into the dynamics equations of motion. The results from calculations with the models showed that ship motions are indeed affected by the flooding and green water events and that these motions can be estimated with the time-domain program. It was also found that for a large ship green water has little effect on ship motions but that it can cause a significant increase in local loads on the weatherdeck and superstructure. In short, the models developed by this thesis along with the LAMP program can be used as a damaged stability prediction tool.

A major problem with running the LAMP 3-D nonlinear formulation (LAMP-4) is the extensive computation time, especially to run a full flooding simulation over a long timeline. Unless ship motions are very large, however, the nonlinear calculation is probably unnecessary. A comparison of calculation results using the nonlinear LAMP-4 formulation and the linear LAMP-2 formulation shows that the LAMP-2 results provide adequate accuracy in the ship motion calculation for estimating damaged stability. For best results with the linear calculation for a flooding simulation, an appropriate mean body boundary position needs to be selected

by careful consideration of the ship's initial and final flooded position. Experience with the hydrodynamic properties of the hull in question would help in determining what body position to linearize about.

Several methods of calculating the relative velocity for the water shipping problem were attempted. It was concluded that the best method was Method III which conserved the wave particle momentum.

6.2 Problems Encountered

6.2.1 Computational Difficulties During Rapid Changes in Mass and Mass Distribution

Time-dependent mass and mass moment of inertia was included in equation 2.45 for the dynamics equations of motion. A backward difference scheme was used to calculate the time-derivative terms. Say $\overline{\Omega(t)}$ stands for either the mass matrix or the mass moment of inertia tensor, then $\frac{d\Omega(i,j,n\Delta t)}{dt} = \frac{\Omega(i,j,n\Delta t) - \Omega(i,j,(n-1)\Delta t)}{\Delta t}$ represents the time-derivative for the i th, j th component of the matrix or tensor. During simulations where these derivative terms were large, for example water shipping with relative elevations greater than about 10 feet or a large flooded volume undergoing sloshing with roll amplitudes greater than 25 degrees, it was found the dynamic solution method became unstable. Changing the time derivative to $\frac{d\Omega(i,j,n\Delta t)}{dt} = \frac{\Omega(i,j,n\Delta t) - \Omega(i,j,(n-2)\Delta t)}{2\Delta t}$ provided more of an averaged estimate for the derivative and sometimes kept the dynamic solution method stable. Still, some calculations with large mass and mass moment of inertia time-derivative values of were unable to be completed due to instability. More elaborate methods of estimating the derivatives were not investigated.

6.2.2 Selection of the Time Discretization for the Flux Difference Splitting method

For a given discretization, the stability of the flux difference splitting method used to solve the water motion on deck problem is a function of the water depth and particle velocity. As either of these quantities becomes too large the scheme can become unstable unless the length of the time step is decreased. Smaller time steps, however, slow the LAMP calculation and make it

computationally expensive to get through a complete damaged scenario or flooding timeline. Also, the maximum relative elevation for water shipping, which governs the green water depth, may not be known prior to completing the calculation. If in this case the maximum relative elevation is underestimated during calculation setup then the calculation may be unstable; if the elevation is overestimated during setup then the time step will be smaller than necessary.

For a large ship where green water has little effect on ship motions, the LAMP calculation could be uncoupled from the green water calculation by running the green water calculation as a post process using data generated by the main LAMP calculation. The LAMP generated data could be analyzed in order to optimally setup the green water post process calculation. Of course, for a small ship in large seas green water will affect motions and the green water calculation should remain coupled with the main LAMP calculation.

6.2.3 Calculating Relative Velocity for the Water Shipping Problem

Accurate calculation of relative velocity for the water shipping problem requires more research. Sea spectrum are typically described using a summation of gravity waves each of which solves the linearized free surface boundary condition and with the wave particle velocities specified on the undisturbed plane of the free surface and below. To accurately calculate the relative velocity when shipping water, the wave particle velocity for the portion of the wave that is instantaneously higher than the ship bulwark or deck edge must be known.

If the water shipping event occurs when the deck edge or bulwark is above the undisturbed free surface, or with large amplitude waves, then linear wave theory may not provide an accurate value for water particle velocity. Shipping water is inherently a nonlinear problem but has been modeled in this thesis with linear assumptions. Stokes expansions, which are nonlinear solutions for plane waves based on systematic power series in the wave amplitude, may be a method of describing the seaway to introduce nonlinear water particle velocity into the water shipping calculation.

Finally, hydraulic flow was used in the relative velocity calculation but this also an approximation of the actual velocities that occur at the wave and deck edge interface. Some water shipping calculations were performed by omitting the hydraulic velocity term but the results did not look very physical. Too little green water mass entered onto the weatherdeck. It is

concluded that in addition to the terms for particle and deck edge velocity a third term such as the hydraulic term is need for accurate relative velocity calculation. However, the hydraulic method may not be the correct way to calculate the term. Use of wave phase or group velocity, or applying dam-breaking results from [29], may provide an alternate method of calculating the third term to give a more accurate water shipping model. Theoretical uncertainties in calculating the relative water velocity explain why the constant C_o must be used in equation 4.30 to adjust theoretical estimates to match experimental results.

6.3 Recommendations for Future Research

Although this research has demonstrated including models for flooding and green water into LAMP so that it can be used as a damaged stability prediction tool, much more work should be done to develop the models. Recommendations include:

- The green water model currently consists of longitudinal strips on the weatherdeck where two-dimensional free surface calculations are performed to solve the water flow on deck problem. This method prevents transverse flow of water which does not allow water to fall off the sides of the weatherdeck. The result is that the calculated green water mass on the ship becomes artificial and remains on the ship longer than it should. A three-dimensional free surface green water model should be developed to correct this condition.
- Some experimentation has been performed on water shipping such as that reported by Grochowalski in [11]. These experiments should be repeated in a computer simulation with the LAMP models in order to validate the models. This work would also help in determining a proper value for the constant in the water shipping mass introduction equation 4.30.
- A rich area for future work is to examine the nonlinear aspects of the water shipping problem and formulate a more theoretical approach for calculating relative velocity in the water shipping problem. The scope of this work should also look at calculation of the free surface elevations when considering the pile-up that occurs from slamming.

- Damaged model testing was reported in references [14], [15], and [16]. Work should be performed to see if these results can be repeated in LAMP simulations.
- Finally, structural loads on the ship while in a damaged condition have not been addressed in this thesis except for illustrating that the local deck loads will increase in the green water problem. The flooding and green water models should be expanded to include effects on main girder and local structural loads.

Appendix A

Moment of Inertia Tensor Calculations

This appendix provides notes on the moment of inertia tensor calculations for a flooded compartment volume. Figure A-1 shows a parallelepiped with sides of length a , b , and c as indicated.

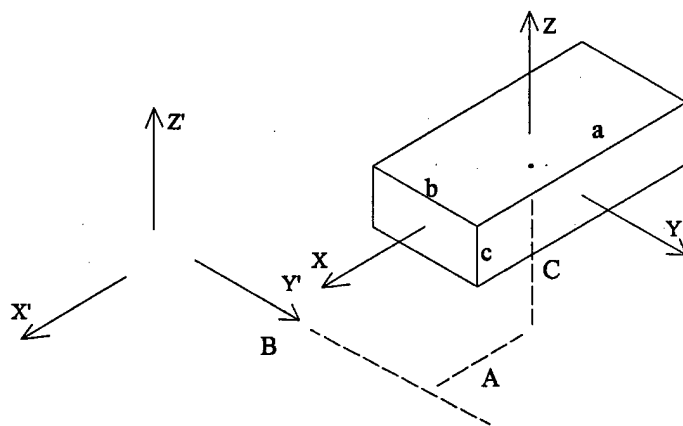


Figure A-1: Parallelepiped

The volume moment of inertia of the parallelepiped about its center is, $I_{xx} = \frac{abc}{12}(b^2 + c^2)$,

$I_{yy} = \frac{abc}{12}(a^2 + c^2)$, and $I_{zz} = \frac{abc}{12}(a^2 + b^2)$. The moment of inertia tensor, \bar{I} , is written as,

$$\begin{bmatrix} I_{xx} & 0 & 0 \\ 0 & I_{yy} & 0 \\ 0 & 0 & I_{zz} \end{bmatrix}$$

The parallel axis theorem can be used to refer \bar{I} to the primed coordinate system in figure A-1. The coordinates (A, B, C) are the center of the parallelepiped in the primed frame. The equation for the parallel axis theorem is

$$\bar{I}' = \bar{I} + abc \begin{bmatrix} B^2 + C^2 & -AB & -AC \\ -AB & A^2 + C^2 & -BC \\ -AC & -BC & A^2 + B^2 \end{bmatrix}$$

If the parallelepiped moment of inertia, \bar{I} , was obtained about a point other than its center, then there would be additional terms in the parallel axis equation.

The rotational transformation of the moment of inertia tensor refers the tensor to a coordinate system that is related to the first through a rotational transformation matrix, \bar{C} . This matrix performs the same function as the euler angle transformation matrix, \bar{L} , discussed in Chapter 2. Say the moment of inertia tensor of a body \bar{I} is referred to the unprimed coordinate system in figure A-2 and \bar{C} is the rotational transformation matrix between the twocoordinate systems. The transformation of \bar{I} is performed by,

$$\bar{I}' = \bar{C}\bar{I}\bar{C}^T$$

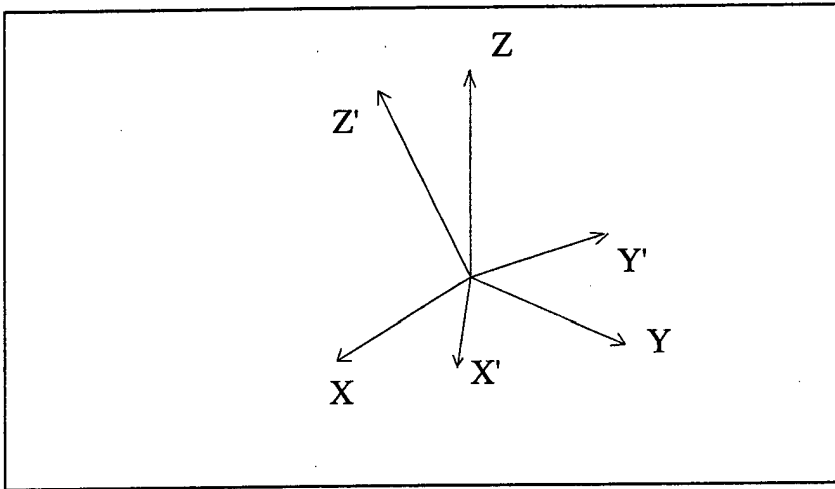


Figure A-2: Rotation of Coordinate Systems

Appendix B

Details of Riemann Problem Calculations

In reference (Stoker), Stoker demonstrates how the Riemann problem may be solved when the fluid is initially at rest on the right-hand side of the dam. In order to use some of the Stoker results in the below calculations, an axis system will be adopted that moves at constant velocity. Use of the Stoker results is justified by showing that the solution to the dam breaking problem is invariant with respect to the moving axis system.

Moving Axis System

Figure B-1 illustrates initial conditions for the Riemann problem in stationary frame y while figure B-2 illustrates the same problem in reference frame y' translating at steady velocity, V_0 .

The two reference frames are related as follows, where c , the wave propagation speed, equals $\sqrt{g\lambda}$.

$$y = y' + V_0 t \quad (\text{B.1})$$

$$V(y', t) = V(y' + V_0 t, t) - V_0 \quad (\text{B.2})$$

$$\lambda(y', t) = \lambda(y' + V_0 t, t) \quad (\text{B.3})$$

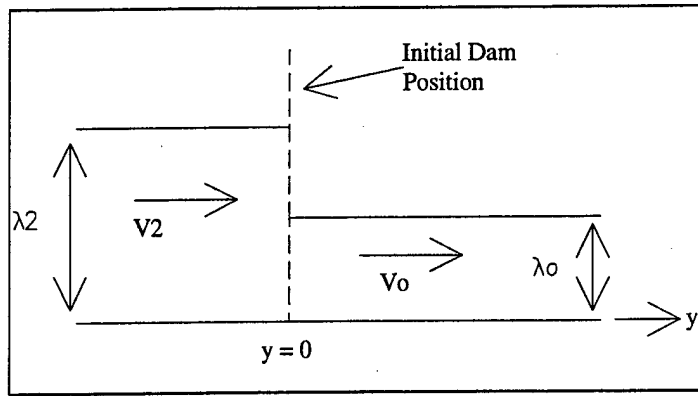


Figure B-1: Initial Conditions for the Riemann Problem

$$c'(y', t) = c(y' + V_0 t, t) \quad (\text{B.4})$$

From reference (stoker) the shallow water wave equations can be formulated in terms of the velocity, V , and propagation speed, c . These equations for the stationary frame are

$$\frac{\partial V}{\partial t} + V \frac{\partial V}{\partial y} + 2c \frac{\partial c}{\partial y} = 0 \quad (\text{B.5})$$

$$2 \frac{\partial c}{\partial t} + 2V \frac{\partial c}{\partial y} + c \frac{\partial V}{\partial y} = 0 \quad (\text{B.6})$$

which can be added or subtracted from each other to form characteristic equations

$$\left\{ \frac{\partial}{\partial t} + (V + c) \frac{\partial}{\partial y} \right\} (V + 2c) = 0 \quad (\text{B.7})$$

$$\left\{ \frac{\partial}{\partial t} + (V - c) \frac{\partial}{\partial y} \right\} (V - 2c) = 0 \quad (\text{B.8})$$

Equations B.7 and B.8 state that the function $(V + 2c)$ is constant for a point moving through the fluid with the velocity $(V + c)$ and that the function $(V - 2c)$ is constant for a point moving through the fluid with the velocity $(V - c)$. There are two sets of curves, C_1 and

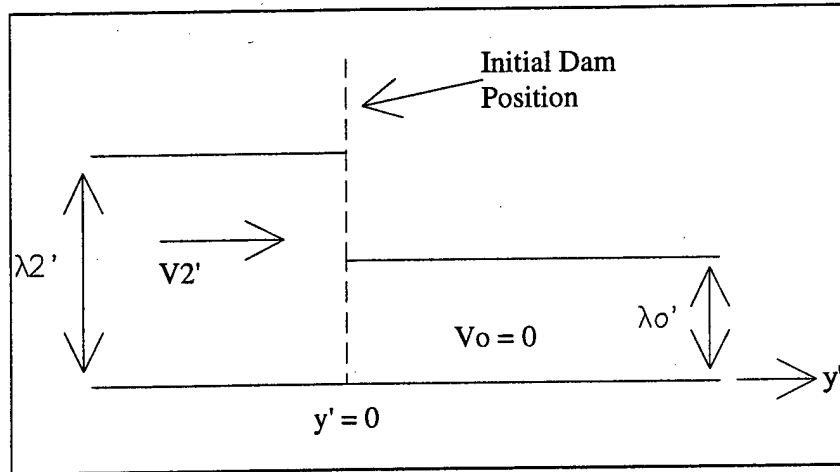


Figure B-2: Initial Conditions for Riemann Problem in Steady Velocity Frame

C_2 called characteristics, which are the solution curves of the ordinary differential equations

$$C_1 : \frac{dy}{dt} = V + c \quad (\text{B.9})$$

$$C_2 : \frac{dy}{dt} = V - c \quad (\text{B.10})$$

Along characteristic C_1 , $V + 2c$ is constant and along C_2 , $V - 2c$ is constant. Similarly, the shallow water wave equations for the translating frame are

$$\frac{\partial V'}{\partial t} + V' \frac{\partial V'}{\partial y'} + 2c' \frac{\partial c'}{\partial y'} = 0 \quad (\text{B.11})$$

$$2 \frac{\partial c'}{\partial t} + 2V' \frac{\partial c'}{\partial y'} + c' \frac{\partial V'}{\partial y'} = 0 \quad (\text{B.12})$$

substituting equations B.2 and B.3 into equations

$$\left[V_0 \frac{\partial V}{\partial y} + \frac{\partial V}{\partial t} + (V - V_0) \frac{\partial V}{\partial y} + 2c \frac{\partial c}{\partial y} \right] \Big|_{y=y'+V_0 t} = 0 \quad (\text{B.13})$$

$$\left[V_0 \frac{\partial c}{\partial y} + \frac{\partial c}{\partial t} + 2(V - V_0) \frac{\partial c}{\partial y} + c \frac{\partial V}{\partial y} \right] \Big|_{y=y'+V_0 t} = 0 \quad (\text{B.14})$$

Equations B.13 and B.14 can be simplified to

$$\frac{\partial V}{\partial t} + V \frac{\partial V}{\partial y} + 2c \frac{\partial c}{\partial y} \Big|_{y=y'+V_0 t} = 0 \quad (\text{B.15})$$

$$2 \frac{\partial c}{\partial t} + 2V \frac{\partial c}{\partial y} + c \frac{\partial V}{\partial y} \Big|_{y=y'+V_0 t} = 0 \quad (\text{B.16})$$

which are the same equations as B.5 and B.6. Thus the translating frame has the same solution curves, characteristics, as the stationary frame which shows the solution to B.5 and B.6 are invariant with respect to axes moving with constant velocity.

Relations From Stoker

The following results from reference (stoker) will be used in the details of the Riemann Problem calculation. Referring

to Figure B-3, for a bore advancing at velocity ξ , the equations for mass and momentum conservation are

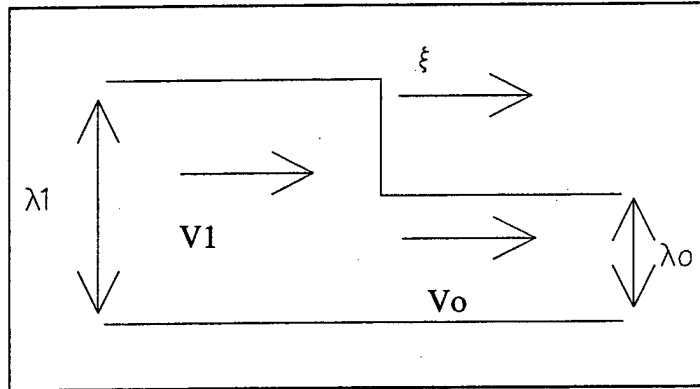


Figure B-3: Advancing Bore

$$\rho \lambda_1 (V_1 - \xi) = \rho \lambda_0 (V_0 - \xi) \quad (\text{B.17})$$

$$\rho \lambda_1 V_1 (V_1 - \xi) - \rho \lambda_0 V_0 (V_0 - \xi) = \frac{1}{2} \rho g (\lambda_0^2 - \lambda_1^2) \quad (\text{B.18})$$

equation B.17 can be solved for the shock speed, ξ

$$\xi = \frac{\lambda_1 V_1 - \lambda_0 V_0}{\lambda_1 - \lambda_0} \quad (\text{B.19})$$

equations B.17 and B.18 can be combined to solve for V_1

$$V_1 = \left[\frac{g(\lambda_0 + \lambda_1)(\lambda_1 - \lambda_0)^2}{2\lambda_0\lambda_1} \right]^{\frac{1}{2}} + V_0 \quad (\text{B.20})$$

When $V_0 = 0$, the following relations can be derived from equations B.17 and B.18

$$\frac{V_1}{c_0} = \frac{\xi}{c_0} - \frac{c_0}{4\xi} \left(1 + \sqrt{1 + 8 \left(\frac{\xi}{c_0} \right)^2} \right) \quad (\text{B.21})$$

$$\frac{c_1}{c_0} = \left[\frac{1}{2} \left(\sqrt{1 + 8 \left(\frac{\xi}{c_0} \right)^2} - 1 \right) \right]^{\frac{1}{2}} \quad (\text{B.22})$$

Calculations for Case I

When $V_2 + 2c_2 > V_0 + 2c_0$, the values for the C_1 characteristics of the high side of the dam and the low side of the dam are discontinuous which forms a shock, represented by ξ' in figure B-4. Velocity and water height values are primed in figure B-4 due to the coordinate translating at steady velocity V_0 .

Curved characteristic C_1 , indicated in figure B-4, is the solution curve where $V_3' + 2c_3'$ is constant. Since C_1 intersects dashed line I in zone 1, then $C_1 = V_1' + 2c_1'$. Therefore $V_3' + 2c_3' = V_1' + 2c_1'$. Also, since C_1 intersects dashed line II in zone 2, then $C_1 = V_2' + 2c_2'$. Therefore $V_3' + 2c_3' = V_2' + 2c_2'$. Then

$$V_1' + 2c_1' = V_2' + 2c_2' \quad (\text{B.23})$$

substituting equation B.21 for V_1' and equation B.22 for c_1' , equation B.23 can be written

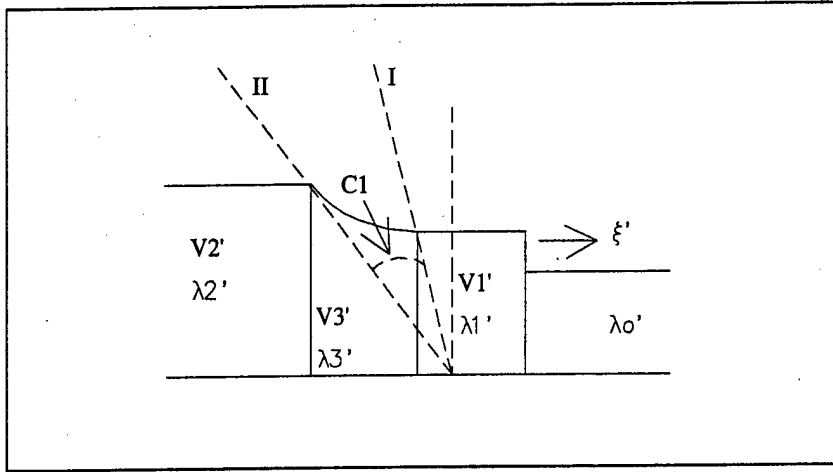


Figure B-4: Case I, Coordinate System Translating at V_0

as

$$\xi' - \frac{c_0'^2}{4\xi'} \left[1 + \sqrt{8 \left(\frac{\xi'}{c_0'} \right)^2 + 1} \right] + 2c_0' \left[\frac{1}{2} \left(\sqrt{8 \left(\frac{\xi'}{c_0'} \right)^2 + 1} - 1 \right) \right]^{\frac{1}{2}} = V_2' + 2c_2' \quad (\text{B.24})$$

next substitute $R = \frac{\xi'}{c_0'}$ into equation B.24

$$R - \frac{1}{4R} \left[1 + \sqrt{8R^2 + 1} \right] + 2 \left[\frac{1}{2} \left(\sqrt{8R^2 + 1} - 1 \right) \right]^{\frac{1}{2}} = \frac{V_2' + 2c_2'}{c_0'} \quad (\text{B.25})$$

After solving equation B.25 for R , the solution for zone 1 can be determined for the fixed axis system by substituting $\xi' = \xi - V_0$, and $V_1' = V_1 - V_0$.

$$\begin{aligned} \xi &= c_0 R + V_0 \\ V_1 &= c_0 \left[R - \frac{1}{4R} \left(1 + \sqrt{8R^2 + 1} \right) \right] + V_0 \\ c_1 &= c_0 \left[\frac{1}{2} \left(\sqrt{8R^2 + 1} - 1 \right) \right]^{\frac{1}{2}} \\ \lambda_1 &= \frac{c_1^2}{g} \end{aligned}$$

There are a fan pattern of straight line characteristics, not shown in figure B-4, that fan

between characteristic *I* and characteristic *II* and pass through characteristic C_1 . On C_1

$$V_3' + 2c_3' = V_2' + 2c_2' \quad (\text{B.26})$$

Also, on the fan of straight characteristics in zone 3

$$\frac{dy'}{dt} = \frac{y'}{t} = V_3' - c_3' \quad (\text{B.27})$$

combining equations B.26 and B.27 to eliminate c_3' gives

$$V_3' = \frac{2}{3} \left(\frac{y'}{t} + \frac{V_2'}{2} + c_2' \right) \quad (\text{B.28})$$

finally determine the zone 3 velocity solution in the fixed axis system by substituting $V_2' = V_2 - V_0$, $V_3' = V_3 - V_0$, and $\frac{y'}{t} = \frac{y}{t} - V_0$.

$$V_3 = \frac{2}{3} \left(\frac{y}{t} - V_0 + \frac{V_2 - V_0}{2} + c_2 \right) + V_0$$

Similar to the solution for V_3 , c_3 can be solved for by combining equations B.26 and B.27 to eliminate V_3' giving

$$c_3' = \frac{1}{3} \left(V_2' + 2c_2' - \frac{y'}{t} \right) \quad (\text{B.29})$$

substituting $\lambda_3' = \frac{(c_3')^2}{g}$ into B.29 gives

$$\lambda_3' = \frac{1}{9g} \left(V_2' + 2c_2' - \frac{y'}{t} \right)^2 \quad (\text{B.30})$$

finally determine the zone 3 height solution in the fixed axis system by substituting $V_2' = V_2 - V_0$, and $\frac{y'}{t} = \frac{y}{t} - V_0$.

$$\lambda_3 = \frac{1}{9g} \left(V_2 + 2c_2 - \frac{y}{t} \right)^2$$

Zone 3 is bounded by characteristic *I* and characteristic *II*. For characteristic *I*, $\frac{dy'}{dt} = V_1' - c_1'$, and for characteristic *II*, $\frac{dy'}{dt} = V_2' - c_2'$. Therefore the zone 3 solution is bounded

by

$$(V_2' - c_2')t < y' < (V_1' - c_1')t \quad (\text{B.31})$$

or converting to the fixed axis system, the zone 3 solution is bounded by

$$(V_2 - c_2)t < y < (V_1 - c_1)t \quad (\text{B.32})$$

The above solution for the zone 3 velocity are for a velocity that increases with increasing y . Thus, the Case I results are only good when $V_2 < V_1$ to allow for an increasing V_3 . If $V_2 > V_1$, a velocity step-down between zones 2 and 1 would form a shock on the left side of the dam. Therefore, after solving for V_1 make the following check to see if $V_2 < V_1$. Equation B.20 is substituted for V_1

$$V_2 < \left[\frac{g(\lambda_0 + \lambda_1)(\lambda_1 - \lambda_0)^2}{2\lambda_0\lambda_1} \right]^{\frac{1}{2}} + V_0 \quad (\text{B.33})$$

If equation B.33 is not met, then shocks form on the left and right-hand sides of the dam and the Riemann problem solution is of Case II, as indicated in figure B-5.

Calculations for Case II

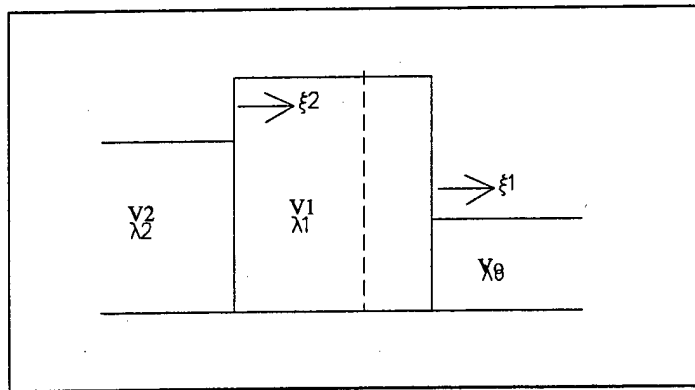


Figure B-5: Case II, Fixed Coordinate System

To solve Case II, equation B.20 must be used for each shock, ξ_1 and ξ_2 .

$$V_1 = \left[\frac{g(\lambda_0 + \lambda_1)(\lambda_1 - \lambda_0)^2}{2\lambda_0\lambda_1} \right]^{\frac{1}{2}} + V_0 \quad (\text{B.34})$$

$$V_2 = \left[\frac{g(\lambda_1 + \lambda_2)(\lambda_2 - \lambda_1)^2}{2\lambda_1\lambda_2} \right]^{\frac{1}{2}} + V_1 \quad (\text{B.35})$$

substituting equation B.34 into equation B.35 for V_1 results in an equation that can be solved for λ_1

$$V_2 - V_0 - \left[\frac{g(\lambda_0 + \lambda_1)(\lambda_1 - \lambda_0)^2}{2\lambda_0\lambda_1} \right]^{\frac{1}{2}} - \left[\frac{g(\lambda_1 + \lambda_2)(\lambda_2 - \lambda_1)^2}{2\lambda_1\lambda_2} \right]^{\frac{1}{2}} = 0 \quad (\text{B.36})$$

once λ_1 is determined then equation B.34 can be used to calculate V_1 . The two shock speeds are found using equation B.19

$$\xi_1 = \frac{\lambda_1 V_1 - \lambda_0 V_0}{\lambda_1 - \lambda_0} \quad \text{and} \quad \xi_2 = \frac{\lambda_2 V_2 - \lambda_1 V_1}{\lambda_2 - \lambda_1} \quad (\text{B.37})$$

Calculations for Case III

The entering argument for case I was that $V_2 + 2c_2 > V_0 + 2c_0$. When this condition is not met, rarefaction waves instead of shock waves occur. For case III, $V_2 + 2c_2 < V_0 + 2c_0$ which can be re-written as $V_0 - V_2 > 2(c_2 - c_0)$ or

$$V_0 - V_2 > 2|c_0 - c_2| \quad (\text{B.38})$$

The solution to case III can be found by analyzing characteristics *I* through *IV*, C_1 , and C_2 as illustrated in figure B-6.

On characteristic C_1 , $V_3 + 2c_3$ is constant. Since this characteristic intersects zones 1 and 2

$$V_2 + 2c_2 = V_1 + 2c_1 \quad (\text{B.39})$$

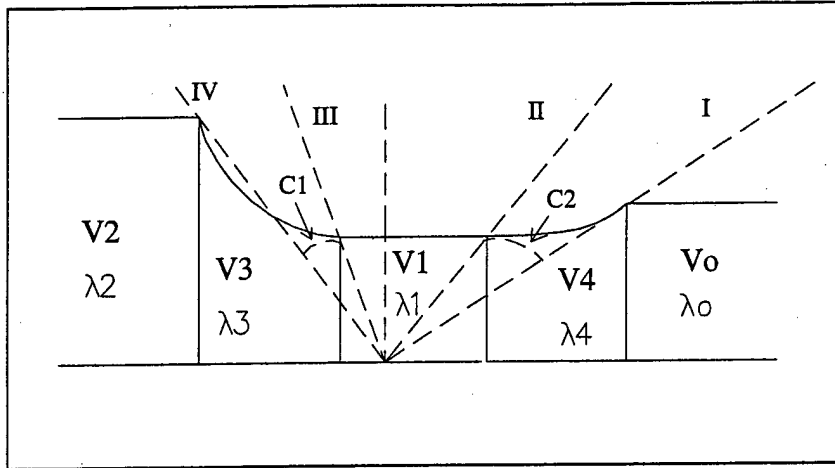


Figure B-6: Case III, Fixed Coordinate System

On characteristic C_2 , $V_4 - 2c_4$ is constant. Since this characteristic intersects zones 1 and 0

$$V_0 - 2c_0 = V_1 - 2c_1 \quad (\text{B.40})$$

adding equations B.39 and B.40 gives

$$V_1 = \frac{V_0 + V_2}{2} + c_2 - c_0 \quad (\text{B.41})$$

subtracting equations B.39 and B.40 gives

$$c_1 = \frac{c_2 + c_0}{2} + \frac{V_2 - V_0}{4} \quad (\text{B.42})$$

since $\lambda_1 = \frac{(c_1)^2}{g}$, equation B.42 can be written as

$$\lambda_1 = \frac{1}{g} \left[\frac{c_2 + c_0}{2} + \frac{V_2 - V_0}{4} \right]^2 \quad (\text{B.43})$$

Zone 3 is solved similarly to the zone 3 solution in case I. There are a fan pattern of straight line characteristics, not shown in figure B-6, that fan between characteristic III and

characteristic *IV* and pass through characteristic C_1 . On C_1

$$V_3 + 2c_3 = V_2 + 2c_2 \quad (\text{B.44})$$

Also, on the fan of straight characteristics in zone 3

$$\frac{dy}{dt} = \frac{y}{t} = V_3 - c_3 \quad (\text{B.45})$$

combining equations B.44 and B.45 to eliminate c_3 gives

$$V_3 = \frac{2}{3} \left(\frac{y}{t} + \frac{V_2}{2} + c_2 \right) \quad (\text{B.46})$$

Similarly, solve for c_3 by combining equations B.44 and B.45 to eliminate V_3 giving

$$c_3 = \frac{1}{3} \left(V_2 + 2c_2 - \frac{y}{t} \right) \quad (\text{B.47})$$

substituting $\lambda_3 = \frac{(c_3)^2}{g}$ into B.47 gives

$$\lambda_3 = \frac{1}{9g} \left(V_2 + 2c_2 - \frac{y}{t} \right)^2 \quad (\text{B.48})$$

Zone 3 is bounded by characteristics *III* and *IV*. For characteristic *III*, $\frac{dy}{dt} = V_1 - c_1$, and for characteristic *IV*, $\frac{dy}{dt} = V_2 - c_2$. Therefore the zone 3 solution is bounded by

$$(V_2 - c_2)t < y < (V_1 - c_1)t \quad (\text{B.49})$$

For Zone 4 there are a fan pattern of straight line characteristics, not shown in figure B-6, that fan between characteristics *I* and *II*. All pass through characteristic C_2 . On C_2

$$V_4 - 2c_4 = V_0 - 2c_0 \quad (\text{B.50})$$

Also, on the fan of straight characteristics in zone 4

$$\frac{dy}{dt} = \frac{y}{t} = V_4 + c_4 \quad (\text{B.51})$$

combining equations B.50 and B.51 to eliminate c_4 gives

$$V_4 = \frac{2}{3} \left(\frac{y}{t} + \frac{V_0}{2} - c_0 \right) \quad (\text{B.52})$$

Similarly, solve for c_3 by combining equations B.50 and B.51 to eliminate V_4 giving

$$c_4 = \frac{1}{3} \left(\frac{y}{t} - V_0 + 2c_0 \right) \quad (\text{B.53})$$

substituting $\lambda_4 = \frac{(c_4)^2}{g}$ into equation B.53 gives

$$\lambda_4 = \frac{1}{9g} \left(\frac{y}{t} - V_0 + 2c_0 \right)^2 \quad (\text{B.54})$$

Zone 4 is bounded by characteristics *I* and *II*. For characteristic *I*, $\frac{dy}{dt} = V_0 + c_0$, and for characteristic *II*, $\frac{dy}{dt} = V_1 + c_1$. Therefore the zone 4 solution is bounded by

$$(V_1 + c_1)t < y < (V_0 + c_0)t \quad (\text{B.55})$$

Calculations for Case IV

If $\lambda_0 = 0$ then the solution consists of solving the single rarefaction illustrated in figure B-7.

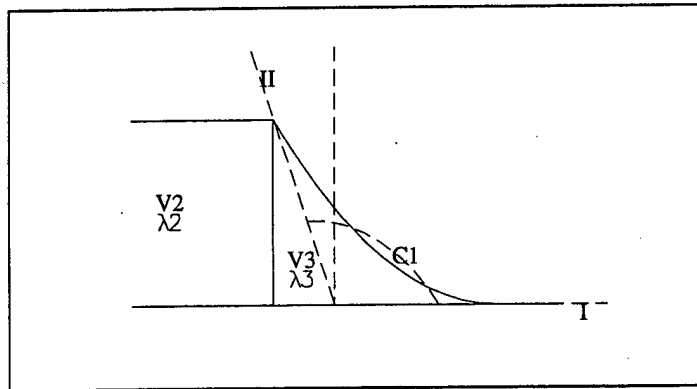


Figure B-7: Case IV, Fixed Coordinate System

The solution to case IV can be found by analyzing characteristics *I*, *II*, and C_1 . There is a fan pattern of straight line characteristics, not shown in figure B-7, that fan between

characteristics *I* and *II* and pass through characteristic C_1 . On C_1

$$V_3 + 2c_3 = V_2 + 2c_2 \quad (\text{B.56})$$

On characteristic *I*, the depth at the water boundary is zero, $c_3 = 0$, so that $V_3 = V_2 + 2c_2$. This means that the boundary of the water moves to the right on the y axis at velocity $V_2 + 2c_2$.

Also, on the fan of straight characteristics in zone 3

$$\frac{dy}{dt} = \frac{y}{t} = V_3 - c_3 \quad (\text{B.57})$$

combining equations B.56 and B.57 to eliminate c_3 gives

$$V_3 = \frac{2}{3} \left(\frac{y}{t} + \frac{V_2}{2} + c_2 \right) \quad (\text{B.58})$$

Similarly, solve for c_3 by combining equations B.56 and B.57 to eliminate V_3 giving

$$c_3 = \frac{1}{3} \left(V_2 + 2c_2 - \frac{y}{t} \right) \quad (\text{B.59})$$

substituting $\lambda_3 = \frac{(c_3)^2}{g}$ into equation B.59 gives

$$\lambda_3 = \frac{1}{9g} \left(V_2 + 2c_2 - \frac{y}{t} \right)^2 \quad (\text{B.60})$$

Zone 3 is bounded by characteristics *I* and *II*. For characteristic *II*, $\frac{dy}{dt} = V_2 - c_2$, and for characteristic *I*, on the y axis, the water boundary moves at $V_2 + 2c_2$. Therefore the zone 3 solution is bounded by

$$(V_2 - c_2)t < y < (V_2 + 2c_2)t \quad (\text{B.61})$$

Calculations for Case V

Case V occurs when the conditions for case III are met but the result for λ_1 in equation B.43 is less than zero. The situation is illustrated in figure B-8. To determine when $\lambda_1 < 0$, use

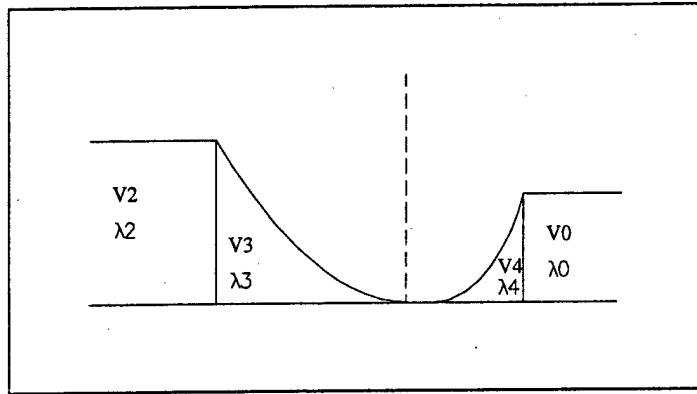


Figure B-8: Case V, Fixed Coordinate System

equation B.43

$$\frac{1}{g} \left[\frac{c_2 + c_0}{2} + \frac{V_2 - V_0}{4} \right]^2 < 0 \quad (\text{B.62})$$

which can be rewritten as

$$V_2 + 2c_2 < V_0 - 2c_0 \quad (\text{B.63})$$

The solution for zone 3 in this case is identical to the solution for zone 3 in case IV. The solution for zone 4 can be developed from characteristics similar to equations B.57 through B.61. The results are

$$V_4 = \frac{2}{3} \left(\frac{y}{t} + \frac{V_0}{2} - c_0 \right) \quad (\text{B.64})$$

$$\lambda_4 = \frac{1}{9g} \left(\frac{y}{t} - V_0 + 2c_0 \right)^2 \quad (\text{B.65})$$

The zone 4 solution is bounded by

$$(V_0 - 2c_0)t < y < (V_0 + c_0)t \quad (\text{B.66})$$

Appendix C

MATLAB Program to Solve Riemann Problem Using the Random Choice Method

```
% MATLAB Program to Solve Riemann Problem Using
% the Random Choice Method
% gravity acceleration constant
g=9.8;
% wave form for testing
ymax=.5;
ymin=-.5;
dely=.01;
jmax=(ymax-ymin)/dely;
% time stuff
delt=0.001;
tfinal=.08;
tmax=tfinal/delt;
% Boundary Conditions (the Riemann Problem Initial Conditions)
vleft=.8;
```



```

hleft=.6;
vright=1;
hright=.2;
% set initial values
for jj=1:jmax
yplot(jj)=ymin+jj*dely-dely/2;
h(jj)=hleft;
v(jj)=vleft;
if yplot(jj)>=0
h(jj)=hright;
v(jj)=vright;
end
end
for tt=1:tmax           % loop for time (t) evolution
y=(-1)^tt*dely*rand/2; % this is the random number for sampling
% each interval
% do random choice 1 cycle
if y <=0                % if random number less than zero, sample to left
for jj=2:jmax+1
if jj == 1
v2=vleft;
lambda2=hleft;
v0=v(jj);
lambda0=h(jj);
end
if jj == jmax+1        % Right hand side BC
v2=v(jj-1);
lambda2=h(jj-1);
v0=vright;
lambda0=hright;

```

```

end
if jj > 1
if jj < jmax+1
v2=v(jj-1);
lambda2=h(jj-1);
v0=v(jj);
lambda0=h(jj);
end
end
% get solution for the intervals Riemann problem
soln=riemann(lambda0,lambda2,v0,v2,y,delt,g);
vnew(jj-1)=soln(2);
hnew(jj-1)=soln(1);
end
end
if y > 0          % if random number > 0, sample to right
for jj=1:jmax
if jj == 1
v2=vleft;
lambda2=hleft;
v0=v(jj);
lambda0=h(jj);
end
if jj == jmax+1
v2=v(jj-1);
lambda2=h(jj-1);
v0=vright;
lambda0=hright;
end
if jj > 1

```

```

if jj < jmax+1
v2=v(jj-1);
lambda2=h(jj-1);
v0=v(jj);
lambda0=h(jj);
end
end
% get solution for the intervals Riemann problem
soln=riemann(lambda0,lambda2,v0,v2,y,delt,g);
vnew(jj)=soln(2);
hnew(jj)=soln(1);
end
end
% set up for next time step
for jj=1:jmax
v(jj)=vnew(jj);
h(jj)=hnew(jj);
end
end          % end time evolution

% This program returns height and velocity for the Riemann problem with
% the initial conditions provided as calling arguments. The height and
% velocity are returned for location y at time t.
function soln=riemann(lambda0,lambda2,v0,v2,y,time,g)
% soln(1)=height, soln(2)=velocity
% Riemann Problem solver
% these are set so that numbers are always returned
soln(1)=lambda2;
soln(2)=v2;
done=0;
if lambda0==lambda2

```

```

if v0 == v2
done=1;
soln(1)=lambda0;
soln(2)=v0;
end
end
c0=sqrt(g*lambda0);
c2=sqrt(g*lambda2);
% case 4 *****
if lambda0 < 0.01* lambda2
done=1;
soln(1)=(1/(9*g))*(v2+2*c2-y/time)^2;
soln(2)=(2/3)*(y/time+v2/2+c2);
if y <= (v2-c2)*time
soln(1)=lambda2;
soln(2)=v2;
end
if y >= (v2+2*c2)*time
soln(1)=0;
soln(2)=0;
end
end
% ***** end case 4 *****
if done == 0
% case 3 and 5 *****
if (v0-v2)> 2*abs(c0-c2)
if (v2+2*c2)>=(v0-2*c0) % case 3
done=1;
v1=(v0+v2)/2+c2-c0;
lambda1=((v2-v0)/4 +(c2+c0)/2)^2/g;

```

```

c1=sqrt(g*lambda1);
if y >=(v0+c0)*time
soln(1)=lambda0;
soln(2)=v0;
end
if y <=(v2-c2)*time
soln(1)=lambda2;
soln(2)=v2;
end
if y > (v2-c2)*time
if y <= (v1+c1)*time
soln(1)=lambda1;
soln(2)=v1;
end
if y <= (v1-c1)*time % in zone 3
soln(1)= (1/(9*g))*(v2+2*c2-y/time)^2;
soln(2)=(2/3)*(y/time+v2/2+c2);
end
end
if y < (v0+c0)*time
if y > (v1+c1)*time % in zone 4
soln(1)= (1/(9*g))*(2*c0-v0+y/time)^2;
soln(2)=(2/3)*(y/time+v2/2-c0);
end
end
else % case 5
done=1;
if y <= (v2+2*c2)*time
soln(1)=(1/(9*g))*(v2+2*c2-y/time)^2;
soln(2)=(2/3)*(y/time+v2/2+c2);

```

```

if y <= (v2-c2)*time
soln(1)=lambda2;
soln(2)=v2;
end
end
if y >= (v0-2*c0)*time
soln(1)=(1/(9*g))*(v0-2*c0-y/time)^2;
soln(2)=(2/3)*(y/time+v0/2-c0);
if y >= (v0+c0)*time
soln(1)=lambda0;
soln(2)=v0;
end
end
if y > (v2+2*c2)*time
if y < (v0-2*c0)*time
soln(1)=0;
soln(2)=0;
end
end
end
end
% end case 3 and 5
end
lambda1=0;
if done == 0
% possible case 1 or 2 *****
R=rootfind(v0,v2,c0,c2);
for n=1:2
if R(n)>0
r=R(n);

```

```

root=sqrt(8*r^2+1);
zee=c0*r+v0;
v1=c0*(r-1/(4*r)*(1+root))+v0;
c1=c0*sqrt(0.5*(root-1));
lambda1=c1^2/g;
end
end
% test dillingham eq 49
if lambda1 ~=0
rhs=sqrt(g*(lambda1+lambda0)*(lambda1-lambda0)^2/(2*lambda1*lambda0));
end
if (v2-v0) < rhs
v1=c0*(r-1/(4*r)*(1+root))+v0;
if y <= (v2-c2)*time
soln(1)=lambda2;
soln(2)=v2;
end
if y > (v2-c2)*time
if y <= (v1-c1)*time
soln(1)=(1/(9*g))*(v2+2*c2-y/time)^2;
soln(2)=(2/3)*((y/time)-v0+(v2-v0)/2+c2)+v0;
end
if y > (v1-c1)*time
if y <= zee*time
soln(1)=lambda1;
soln(2)=v1;
end
if y > zee*time
soln(1)=lambda0;
soln(2)=v0;

```

```

end
end
end
% case 2
else
% L returns lambda 1 (Dillingham eq (55))
lambda1=rootfind1(v0,v2,c0,c2,g);
v1=v0+sqrt(g*(lambda0+lambda1)*(lambda1-lambda0)^2/(2*lambda0*lambda1));
zee1=0;
if lambda1~=lambda0
zee1=(lambda1*v1-lambda0*v0)/(lambda1-lambda0);
end
zee2=0;
if lambda2~=lambda1
zee2=(lambda2*v2-lambda1*v1)/(lambda2-lambda1);
end
if y >= zee1*time
soln(1)=lambda0;
soln(2)=v0;
end
if y < zee1*time
if y > zee2*time
soln(1)=lambda1;
soln(2)=v1;
end
end
if y <= zee2*time
soln(1)=lambda2;
soln(2)=v2;
end
end

```


end

% ** end case 1 or 2 *****

end

Bibliography

- [1] Alcrudo, F., Garcia-Navarro, P. and Saviron J., "Flux Difference Splitting for 1-D Open Channel Flow Equations," *International Journal for Numerical Methods in Fluids*, Vol. 14, 1009-1018 (1992).
- [2] Anderson, T. J. Development of a SIMSMART Based, Progressive Flooding Tool. Master's Thesis, Department of Mechanical Engineering, Naval Postgraduate School, March 1999
- [3] Caglayan, I. and Storch, R.L., "Stability of Fishing Vessels with Water on Deck," *Journal of Ship Research*, Vol. 26, No. 2, June 1982.
- [4] Chorin, A.J., "Random Choice Solution of Hyperbolic Systems," *Journal of Computational Physics*, Vol. 22, 517-533 (1976).
- [5] DDS 079-1, Design Data Sheet - Stability and Buoyancy of US Naval Surface Ships, Naval Ship Engineering Center, 1 August 1975.
- [6] Dillingham, J., "Motion Studies of a Vessel with Water on Deck," *Marine Technology*, Vol. 18, No.1, January 1981.
- [7] A. Engle, W. Lin, N. Salveson, and Y. Shin. Application of 3-D Nonlinear Wave Load and Structural Response Simulations in Naval Ship Design. *Naval Engineers Journal*, pages 253-268, May 1997.
- [8] Fang, Ming-Chung., Ming-Ling Lee and Chwang-Kuo Lee, "Time Simulation of Water Shipping for a Ship Advancing in Large Longitudinal Waves," *Journal of Ship Research*, Vol. 37, No. 2, June 1993.

- [9] Gillmer, T. C. and Bruce Johnson, 1982. "Introduction to Naval Architecture," Annapolis: Naval Institute Press.
- [10] Glimm, J., "Solutions in the Large for Nonlinear Hyperbolic Systems of Equations," Communications on Pure and Applied Mathematics, Vol. 18, 1965.
- [11] Grochowalski, S., Hsiung, C.C. and Huang, Z.J., "Theoretical Modeling of Ship Motions and Capsizing in Large and Steep Waves," SNAME Transactions, Vol. 106, 1998.
- [12] Huang, Z.J. and Hsiung, C.C., "Nonlinear Shallow Water Flow on Deck," Journal of Ship Research, Vol. 40, No. 4, December 1996.
- [13] Jones, A.F. and Hulme, A., "The hydrodynamics of Water on Deck," Journal of Ship Research, Vol. 31, No. 2, June 1987.
- [14] Jones, Harry D., "DD963 Intact and Damaged Stability in Beam Waves and Wind," David Taylor Research Center, Ship Hydromechanics Department, Bethesda, Md., DTRC/SHD-1360-01, September 1991.
- [15] Jones, Harry D., "DD993 Intact and Damaged Stability in Beam Waves and Wind," David Taylor Research Center, Ship Hydromechanics Department, Bethesda, Md., DTRC/SHD-1360-02, October 1991.
- [16] Jones, Harry D., "DDG-51 Intact and Damaged Stability in Beam Waves and Wind," David Taylor Research Center, Ship Hydromechanics Department, Bethesda, Md., DTRC/SHD-1360-03, January 1992.
- [17] Lewis, E. V., ed., *Principles of Naval Architecture*. New Jersey: SNAME 1988.
- [18] LeConte, Joseph N., *Hydraulics*, McGraw-Hill, New York.
- [19] Lin, Woei-Min and Dick K.P. Yue. Numerical Solutions for Large-Amplitude Ship Motions in the Time Domain. In Proc. Eighteenth Symposium on Naval Hydrodynamics, 1990.
- [20] Lin, Woei-Min, Michael J. Meinhold, Nils Salveson, and Dick K.P. Yue. Large-Amplitude Motions and Wave Loads for Ship Design. In Proc. Twentieth Symposium on Naval Hydrodynamics, 1994.

- [21] Lin, Woei-Min, Michael J. Meinhold, Kenneth M. Weems, Sheguang Zhang, and Marian H.C. WEems. *User's Guide to the LAMP System*. Science Applications International Corporation, Ship Technology Division, 134 Holiday Court, Suite 318, Annapolis, MD 21401, USA, current edition, July 1999. SAIC Report 96/1040.
- [22] Pantazopoulos, M.S. and Adey, B.H., "Three Dimensional Shallow Water Waves in an Oscillating Tank," in *Proceedings*, American Society of Civil Engineers Conference on Coastal Hydrodynamics, University of Delaware, Newark, Del., June 28-July1, 1987.
- [23] Pantazopoulos, M.S., "Three-Dimensional Sloshing of Water on Decks," *Marine Technology*, Vol. 25, No.4, October 1988.
- [24] Report of the Ship Operational Characteristics Study on the Operational Characteristics of the Surface Combatant of the Year 2010, Chief of Naval Operations (OP-03K), Washington D.C., 26 April 1988.
- [25] Sarchin, T. H. and L. L. Goldberg, "Stability and Buoyancy criteria for U.S. Naval Surface Ships," *SNAME Transactions*, Vol. 70, 1962.
- [26] Shin, Y.S., J.S.Chung, W.M.Lin, S. Zhang, and A. Engle. Dynamic Loadings for Structural Analysis of Fine Form Container Ship Based on a Non-Linear Large Amplitude Motions and Load Method. In Proc. SNAME Annual Meeting, pages 4.1 - 4.24, Ottawa, Canada, October 1997. SNAME.
- [27] Sod, Gary A., "A Numerical Study of a Converging Cylindrical Shock," *Journal of Fluid Mechanics*, Vol. 83, Part 2, 1977.
- [28] Steger, J. L. and Warming, R.F., "Flux Vector Splitting of the Inviscid Gasdynamic Equations with Application to Finite-Difference Methods," *Journal of Computational Physics*, 40, 263-293 (1981).
- [29] Stoker, J. J., *Water Waves*, Interscience, New York, 1957
- [30] Stoker, J. J. 1948 The formation of breakers and bores. *Communications on Pure and Applied Mathematics*, 1, 1-87.

[31] Surko, S. W., "An Assessment of Current Warship Damaged Stability Criteria," *Naval Engineers Journal*, May 1994.

[32] Yanenko, N.N., *The Method of Fractional Steps*. Springer-Verlag, New York, 1971.